Title

WITHDRAWN: Dual targeting of mitochondrial Lon peptidase 1 and chymotrypsin-like protease by small molecule BT317, as potential therapeutics in malignant astrocytomas

Journal

bioRxiv, 4(05-02)

Authors

Douglas, Christopher
Jain, Shashi
Lomeli, Naomi
et al.

Publication Date

2024-05-23

DOI

10.1101/2023.04.13.536816

Discovery and Validation of Novel LonP1 and Proteasome Inhibitor in IDH1-R132H Malignant Astrocytoma Models

Christopher Douglas[1], Naomi Lomeli[2], Javier Lepe[1], Kaijun Di[2], Nitesh Kumar Nandwana[5], Adil Shareef Mohammed[5], Thao Vu[2], James Pham[2], Maria Cristina Kenney[3], Bhaskar Das[4,5]*, Daniela A. Bota[1,2,6]*

1 Department of Pathology & Laboratory Medicine, University of California Irvine, Irvine, CA, USA (C.D., D.A.B.)
2 Department of Neurology, University of California Irvine, Irvine, CA, USA (K.D., N.L., T.V., J.P.)
3 Department of Ophthalmology Research, University of California Irvine, Irvine, CA, USA (M.C.K.)
4 Arnold & Marie Schwartz College of Pharmacy & Health Sciences, Long Island University – Brooklyn, NY, USA (N.K.D, B.D.)
5 Department of Pharmacology, Long Island University – Brooklyn, NY, USA (B.D.)
6 Chao Family Comprehensive Cancer Center, University of California Irvine, Irvine, CA, USA (D.A.B.)

***Co-Corresponding Authors:** Daniela A. Bota, M.D., Ph.D.
University of California Irvine, Sprague Hall B200,
Irvine, CA 92697-4475, USA
Phone: (949) 824-7377
Fax: 714-456-6894
Email: dbota@hs.uci.edu

Bhaskar Das, Ph.D.
Long Island University – Brooklyn, 75 DeKalb Avenue, HS-610,
Brooklyn, NY 11201-5497
Phone: (718) 488-1471
Fax: 718-780-4586
E-mail: Bhaskar.Das@liu.edu

Funding: This work was supported by the National Institute of Neurologic Diseases and Stroke Award (NINDS/NIH) [NS109423] to DAB and BD. This work was also supported by the NINDS/NIH Award [NS111303], the National Center for Advancing Translational Sciences (NCATS/NIH) Award [UL1 TR001414], the UCI American Cancer Society Institutional Grant [ACS/IRG – 98-279- 07], the Ruth L. Kirschstein National Research Service T32 Award [2T32CA009054-41 (MPI)] and the UCI Cancer Center Award [P30CA062203] from the National Cancer Institute to DAB. *The content is solely the responsibility of the authors and does not necessarily represent the official views of the National Institutes of Health.*

Conflict of Interest: The authors have no conflicts of interest to disclose.

Authorship Statement: Conception and design of this work: DAB, BD, CD, KD, and NL. Inhibitor synthesis and design: BD and NKD. Brain mass spectrometry measurements: Cyprotex and Biotechnology Innovation and Optimization Center. Data collection, analysis, and interpretation: CD and DAB. All the authors critically reviewed and approved the final manuscript.

Manuscript Word Count: Abstract: 249; Importance of Study: 144; Text: 6257; References: 1777; Figure Legend: 558.

Graphical Abstract

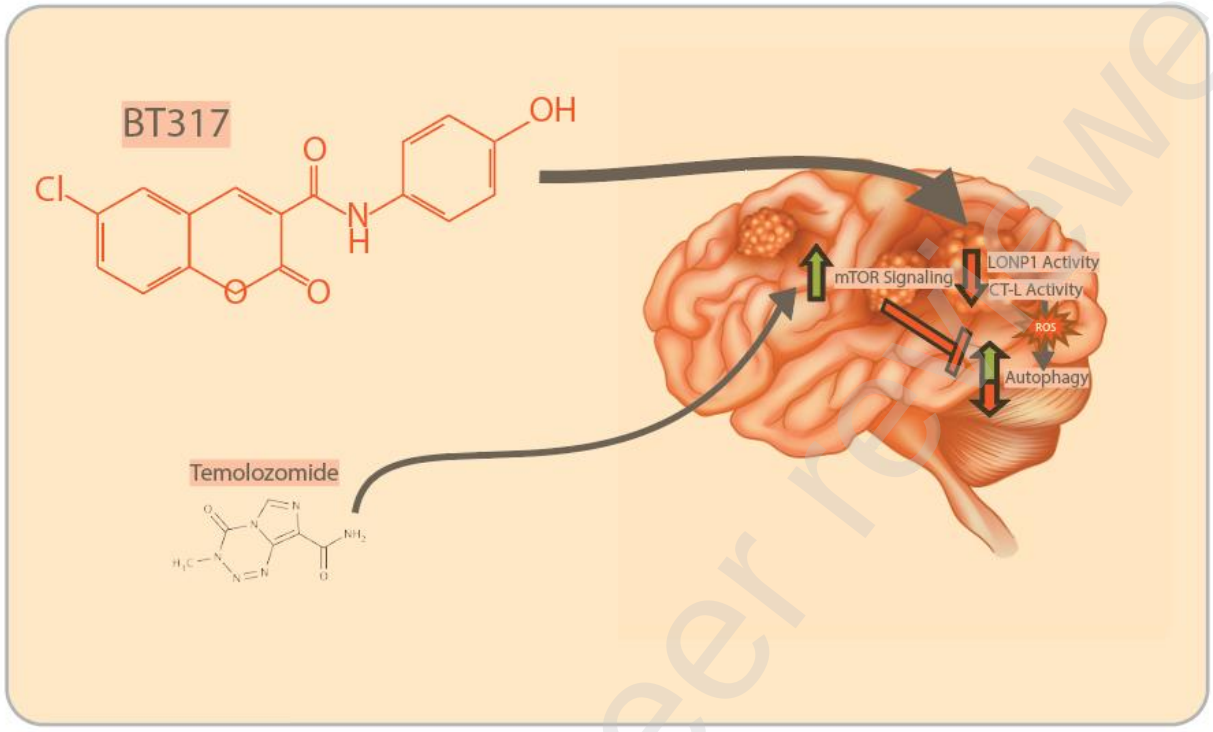

Abstract

Malignant astrocytomas are aggressive glioma tumors that have poor prognosis and limited treatments available following recurrence. These tumors are characterized by extensive hypoxia-induced, mitochondria-dependent changes such as glycolytic respiration, increased chymotrypsin-like (CT-L) proteasome activity, decreased apoptosis, and increased invasiveness. Mitochondrial Lon Peptidase 1 (LonP1) is an ATP-dependent protease directly upregulated by hypoxia-inducible factor 1 alpha (HIF-1α). Both LonP1 expression and CT-L proteasome activities are increased in gliomas and are associated with a high tumor grade and poor patient survival. Recently, dual LonP1 and CT-L inhibition has been found to exhibit synergy against multiple myeloma cancer lines.

We now report that dual LonP1 and CT-L inhibition has synergistic toxicity in IDH mutant astrocytoma when compared to IDH wildtype glioma, due to increased reactive oxygen species (ROS) generation and autophagy. A novel small molecule, BT317, was derived from coumarinic compound 4 (CC4) using structure-activity modeling and was found to inhibit both LonP1 and CT-L proteasome activity and subsequently induce ROS accumulation and autophagy-dependent cell death in high-grade IDH1 mutated astrocytoma lines. *In vitro*, BT317 also had enhanced synergy with the commonly used chemotherapeutic temozolomide (TMZ), which blocked BT317-induced autophagy. This novel dual inhibitor was selective to the tumor microenvironment and demonstrated therapeutic efficacy both as a single agent and in combination TMZ in IDH mutant astrocytoma models. We show that BT317, a dual LonP1, and CT-L proteasome inhibitor exhibited promising anti-tumor activity and could be a promising candidate for clinical translation in the space of IDH mutant malignant astrocytoma therapeutics.

Data Access Statement: Research data supporting this publication are as presented in the manuscript.

Keywords: IDH mutant astrocytoma, Glioblastoma, LonP1, CT-L proteosome, BT317

Highlights

1. The novel compound BT317 acts as a LonP1 and chymotrypsin-like proteasome inhibitor
2. LonP1 and CT-L proteasome inhibition drives ROS production in IDH mutant astrocytoma
3. LonP1 and CT-L proteasome inhibition drives autophagy in IDH mutant astrocytoma
4. BT317 shows blood-brain barrier permeability and has low normal tissue toxicity
5. BT317 synergizes with the first-line chemotherapy agent TMZ

Importance of Study

Malignant astrocytomas (IDH mutant astrocytomas grade 4 and IDH wildtype glioblastoma) have poor clinical outcomes, and novel treatments are needed to limit recurrence and improve overall survival. These tumors have a malignant phenotype that is mediated by altered mitochondrial metabolism and adaptation to hypoxia. Here, we present evidence that the small-molecule inhibitor BT317, with a dual Lon Peptidase 1 (LonP1) and chymotrypsin-like (CT-L) inhibition profile, can be effectively used to induce increased ROS production and autophagy-dependent cell death in clinically relevant, IDH mutant malignant astrocytoma, patient-derived orthotopic models. BT317 showed strong synergy with the standard of care, temozolomide (TMZ), in the IDH mutant astrocytoma models. This could lead to the development of dual LonP1 and CT-L proteasome inhibitors as novel therapeutic strategies for IDH mutant astrocytoma and provide insight for future clinical translation studies in combination with the standard of care.

1. Introduction

Malignant astrocytomas are one of the most aggressive primary and secondary brain tumors, with a three-year expected survival rate following surgical resection, radiation, and chemotherapy. Recurrence is certain after the initial treatment, and there is currently no proven therapy to significantly prolong survival after tumor recurrence[1,2]. The current standard of care, temozolomide (TMZ, temodar), an alkylating agent, provides a median survival advantage of 2.5 months when added to surgery and radiation therapy[3]. The use of Tumor-Treating Fields (TTFields, Optune) further increases this survival advantage by 4 months[4]. Despite significant efforts and numerous past and ongoing clinical trials utilizing small molecule inhibitors such as the STAT3 inhibitor WP1066, EGFR inhibitors, Dopamine Receptor D2 antagonists (ONC201), and new immunotherapy checkpoint inhibitor approaches such as pembrolizumab, nivolumab and ipilimumab, the development of safe and efficacious therapies for malignant astrocytomas has been slow. In the past 16 years, only three therapies (TMZ, bevacizumab, TTFields) have been approved for the treatment of astrocytomas[5]. Thus, there is an urgent need to develop alternative therapeutic strategies.

Malignant astrocytomas are increasingly classified based on their genetic and epigenetic profiles[6]. Less than 10% of grade 4 astrocytomas express isocitrate dehydrogenase 1 or 2 (IDH1/2) mutations, which are associated with an improved response to treatment and prognosis as compared with the IDH wildtype tumors[7]. Based on these biologic and survival differences, the most recent WHO glioma classification excludes tumors with an IDH mutation from being classified as GBM and refers to such tumors as astrocytoma grade 4, IDH mutant[8]. Even though the presence of the IDH mutations predict a better

outcome, the survival of patients with grade 4 IDH mutated astrocytoma treated with the standard therapy (radiation and TMZ) is still only 31 months[9]. The presence of the IDH mutation (>90% are IDH1-R132H) can drive tumorigenesis[10] at the cost of impairing the mitochondrial electron transport chain in cellular mitochondria, increasing ROS production, and creating increased vulnerability to pro-oxidative and apoptotic signals[11]. Direct targeting of the IDH1 mutation using specific inhibitors has proven successful in other malignancies, notably IDH1-mutant Acute myelogenous leukemia, but had limited results in IDH1 mutant malignant astrocytoma, and there is a great need to develop more targeted strategies for this tumor type.

The invasive phenotype of malignant astrocytomas is partly mediated by overexpression of the transcriptional activator hypoxia-inducible factor 1 alpha (HIF-1α). HIF-1α contributes to the hypoxia-driven maintenance of glioma stem cells (GSCs)[12] by supporting self-renewal[13], angiogenesis[14], increased invasiveness[15], and high levels of genetic instability. The latter contributes to tumor heterogeneity and presents a major challenge in devising novel therapeutic strategies for its treatment[16]. There are hundreds of gene targets in the HIF-1α signaling pathway and the nuclear-encoded Lon Peptidase 1 (LonP1) is directly upregulated by HIF-1α[17]. LonP1 is an ATP-dependent protease that regulates mitochondrial homeostasis through three main functions: (1) proteolytic degradation of mitochondrial proteins[17], (2) protein chaperone[18], and (3) mitochondrial DNA (mtDNA)-binding protein[19]. LonP1 overexpression is a poor prognostic factor that promotes invasion and metastasis in multiple cancers, including colorectal[20], melanoma[20] and oral cancer[21]. Our previous results showed that LonP1 is overexpressed in astrocytomas and its elevated expression levels are associated with high tumor grade and poor survival[22]. Furthermore, LonP1 knockdown in established human glioma lines, D-54 MG and U-251 MG, reduced cell viability under normal conditions, and drastically impaired survival under hypoxic conditions[22]. This is concomitant with a decrease in mitochondrial respiration. Notably, LonP1 pharmacological inhibition using the coumarinic compound 4 (CC4)[23] inhibited glioma cell proliferation and synergistically enhanced the therapeutic efficacy of TMZ, *in vitro*[22].

There is difficulty in the generation of specific LonP1 inhibitors[23], which is attributable to its structural similarities with other known proteases and the proteasome[24]. Most LonP1 inhibitors exhibit dual inhibition of LonP1 and the proteasome[23]. Targeting specifically the chymotrypsin-like (CT-L) proteasome activity may be beneficial, as it plays an important role in tumor cell survival[25] and treatment resistance[26]. Dual inhibition of LonP1 and the CT-L proteasome activity could be potentially beneficial as it could offer additional therapeutic benefits compared with targeting either protease activity alone. Recent work in multiple myeloma has demonstrated the strong synergy with LonP1 and CT-L proteasome inhibition[27], using specific inhibitors previously shown to have no cross activity, and to target only LonP1, Bardoxolone methyl (CDDO-ME)[28,29], and the CT-L proteasome activity, carfilzomib (CFZ)[30]. Bortezomib (BTZ) exhibits dual LonP1 and CT-L inhibition and possesses a boronic acid group that can transform into a boronate ester when exposed to reactive oxygen species (ROS)[31]; however, it has poor blood-brain barrier (BBB) permeability[32]. In the subcutaneous U-87 MG and U-251 MG glioma models, BTZ was found to sensitize the glioma tumors to TMZ by suppressing FOXM1-mediated treatment resistance[33]. This study did not use patient-derived lines and resorted to using a subcutaneous model instead of an orthotopic xenograft model. In this study, we present BT317, a derivative of CC4[22,23] and a dual LonP1 and CT-L inhibitor. We assessed its LonP1 protease and proteasome inhibition profiles. We then investigated the efficacy and feasibility of the lead compound BT317 as a single agent and in combination with TMZ as a therapeutic

strategy for specifically IDH mutated malignant astrocytomas, including in two separate IDH1-R132H patient-derived, orthotopic xenograft models.

2. Methods

2.1. Ethics Statement

All astrocytoma tumor specimens were collected under institutional review board approved protocols from patients who underwent surgical tumor resection at the University of California Irvine Medical Center. The neuropathological review was completed by a specialized neuropathologist. All patient-derived samples were deidentified. All animal studies were performed in accordance with the guidelines established by the Institutional Animal Care and Use Committee (IACUC) at the University of California Irvine.

2.2. Synthesis of small molecule BT317 and related compounds

Synthesis of BT317 was initiated using compound **D** (methyl 6-chloro-2-oxo-2H-chromene-3-carboxylate) (**Fig. 1A**). Compound **D** was then synthesized from Compound **A** using the outlined process by first adding 5-chlorosalicyclaldehyde (A, 1.55 g, 10 mM) to CH_3CN (5 mL) in a 35 mL reaction tube. Dimethylmalonate (**B**) (1.45 g, 11 mM) and ethyl piperdine-3-carboxylate (**C**) (15 mg, 10 mol%) in 15 mL of CH_3CN were added. The resulting reaction mixture was stirred at room temperature for 24 h. After the evaporation of CH_3CN, the crude reaction mixture was purified by silica gel chromatography to give a white solid **D** (1.6 g, 60%). Basic hydrolysis of compound **D** was performed to produce Compound **E** acid (6-chloro-2-oxo-2H-chromene-3-carboxylic acid). Acid synthesis was initiated by adding methyl 6-chloro-2-oxo-2H-chromene-3-carboxylate D (1.0 g, 4.2 mM) in ethanol to sodium hydroxide (10% w/v in 20 mL ethanol). The mixture was stirred under reflux for 24 h. After the completion of the reaction, the mixture was cooled to room temperature and diluted with 10% HCl. The solid precipitated out and was isolated and washed with water, yielding compound **E** (white solid, 80% yield). Using compound **E**, we further derivatized to amide (BT173) using a simple amide coupling reaction in the presence of coupling reagents. The 6-chloro-2-oxo-2H-chromene-3-carboxylic acid **E** (1.0 mM) was dissolved in dichloromethane (DCM) (3 mL) in a 35 mL reaction tube. Then 4-hydroxy aniline (1.1 mM) and DCC (1.2 mM) were added. The resulting reaction mixture was stirred at room temperature for 24 h. The reaction was then quenched with a saturated aqueous NaOH solution and extracted with DCM (10 × 3 mL). The combined organic layers were dried over Na_2SO_4 and then filtered. After evaporation of the organic solvent, the residue was purified by silica gel chromatography to obtain BT317, 6-Chloro-N-(4-hydroxyphenyl)-2-oxo-2H-chromene-3-carboxamide (**Fig. 1B;** white solid, 78% yield). The reagents used for the synthesis were purchased from Fisher Scientific. The structure was confirmed by nuclear magnetic resonance (NMR) and proton, carbon, and mass spectrometry, and the purity of the compound was determined by HPLC. The lead compound, BT317, was evaluated using NMR as follows: 1H NMR (500 MHz, DMSO-d6) δ 10.44 (s, 1H), 9.43 (s, 1H), 8.87 (s, 1H), 8.16 (d, J = 2.5 Hz, 1H), 7.82 (dd, J = 8.8, 2.6 Hz, 1H), 7.61 (d, J = 8.9 Hz, 1H), 7.53 (d, J = 8.5 Hz, 2H), 6.78 (d, J = 8.4 Hz, 2H). 13C NMR (125 MHz, DMSO) δ 160.0, 158.8, 154.2, 152.4, 145.7, 134.2, 133.5, 129.5, 129.0, 121.6, 121.2, 119.9, 118.2, 115.3. HRMS (ESI) was calculated for $C_{16}H_{11}ClNO_4$ (M.W. = 316.0371) and 316.0607 [M + H]+.

2.3. Primary and Established Cell Lines

Primary Glioma/Astrocytoma Stem Cell Cultures (GSC)

Patient-derived GSC were isolated from surgical astrocytoma samples in the laboratory of Dr. Daniela A. Bota (DAB), using a previously established method[34]. All GSC cultures were maintained as non-adherent neurospheres in Neurobasal medium (Thermo Fisher; 12349015) supplemented with 20 µg/mL EGF (Thermo Fisher; PHG0313), 20 µg/mL FGF (Thermo Fisher; PHG0023), B27 (Life Technologies; 12587010), GlutaMAX (Thermo Fisher; 35050061), 5 mM sodium pyruvate (Thermo Fisher; 11360070), and antibiotics (Thermo Fisher; 15070063, 15290018). The patient-derived GSC lines included DB70, DB76, DB77, DB81, and 83MES. The patient-derived 83MES line was a kind gift from Dr. Ichiro Nakano at the University of Alabama at Birmingham.

Established Human Glioma Cell Lines

Five established human glioma cell lines, U-251 MG, D-54 MG, and U-87 MG, and the pediatric CHLA-200, were maintained in DMEM/F-12 medium (Corning; 10-090-CV) containing 292 µg/ml glutamine, 1% penicillin/streptomycin (Thermo Fisher; 15070063), and 10% FBS (Invitrogen; 10371-029). All the cell cultures were maintained at 37°C and 5% CO_2 in a humidified incubator.

Normal Cell Lines

The human mammary gland epithelial adherent non-tumorigenic cell line MCF-10A was maintained in DMEM/F-12 medium containing 0.5 mg/mL hydrocortisone, 20 ng/mL hEGF, 100 ng/mL cholera toxin, 1% penicillin/streptomycin, and 5% horse serum (Life Technologies; 26050-070). The human lung fibroblast line HPF242 was maintained in DMEM/F-12 containing 10% FBS and 1% penicillin/streptomycin. All the cell cultures were maintained at 37°C and 5% CO_2 in a humidified incubator. Unlisted reagents were purchased from Sigma-Aldrich and Thermo Fisher Scientific.

2.4. XTT Viability Assay

All established and patient-derived astrocytoma cell lines were seeded at a density of 10,000 cells per well in a 96-well plate (n = 4 replicates per condition). The following day, equal volumes of synthesized inhibitors dissolved in DMSO were added to each well at the specified concentrations (0.1-1000 µM). For the synergy experiments, BT317 was added at specified concentrations with a fixed and specified TMZ concentration. After 72 h, 100 µL volume was removed from each well, and 75 µL of a pre-filtered solution of 1 mg/mL XTT sodium salt (Alfa Aesar, 111072-31-2) and 20 µL/mL XTT activator (Trevigen, 4891-025-02) dissolved in PBS (pH 7.4; Gibco; 10010-023) was added. After 4 h, the absorbance was measured at 490 nm using a SpectraMax Plus 384 microplate reader. GraphPad was then used to perform a log transformation and generate a nonlinear regression curve to calculate IC_{50} viability. The Biochemically Intuitive Generalized Loewe Model (BIGL) was used to determine agonism or antagonism (https://cran.r-project.org/web/packages/BIGL)[35].

2.5. Reactive Oxygen Species Assay

The DB70 line was plated and incubated for 12 h prior to starting treatment. CellROX™ Orange Reagent (Thermo Fisher, C10443) was then added at a working concentration of 5 µM for 30 minutes. After several 1X PBS washes, the cell samples were replated and then imaged using a 20X objective on a Keyence BZ-X810 Widefield Microscope.

2.6. Colony Forming Assay

The DB70 line was treated for 24 h, then plated on 24-well PDL-coated plates for 10 days with partial medium changes at days 4 and 7. Samples were fixed on day 10 with 4% paraformaldehyde for 30 minutes prior to labeling with DAPI in 0.3% Triton 1X PBS. After additional 1X PBS washes, the plates were imaged using a 4X objective on a Keyence BZ-X810 Widefield Microscope.

2.7. Western Blotting

Cell culture samples were exposed to BT317 for 1, 4, 8, and 72 h prior to lysis with RIPA lysis buffer containing 1 mM PMSF, 1 mM Na_3VO_4, and a protease inhibitor cocktail (Sigma, P8340-1ML). The protein concentration was standardized using the DC Protein Assay (Bio-Rad, 500-0114) with a SpectraMax Plus 384 microplate reader. A Precision Plus Protein Kaleidoscope™ ladder (Bio-Rad, 161-0375) and approximately 20 µg of sample were loaded onto each well and run on a Mini Protean TGX Gel (Bio-Rad, 456-1046) before being transferred to an Immobilon Transfer Membrane (Millipore, IPVH08130). The membranes were probed with the indicated primary antibodies and the appropriate secondary antibodies. The primary and secondary antibodies used were 1:2000 LonP1 (Proteintech, 15440-1-AP), 1:1000 Aconitase2 (Abcam, ab71440), 1:1000 LC3B (Cell Signaling Technology, 2775S), FOXM1 (Millipore Sigma, SAB1412254-100UG), C-MET (Fisher Scientific, MAB3729), TFAM (Fisher Scientific, PA5-80107) 1:2000 B-Actin (Novus Biologicals, NB600-501), 1:1000 p-AKT (Abcam, ab192623-100ul), 1:10,000 goat anti-mouse IgG F(ab')2 (Enzo Life Sciences, ADI-SAB-100-J), and 1:3,000 IgG (H+L) Goat anti-Rabbit HRP (Invitrogen, 32460); these were used according to the manufacturer's recommendations and diluted in TBST with 3% BSA. Chemiluminescence was visualized using Amersham™ ECL™ Prime western blotting Detection Reagent (GE Healthcare, RPN2232) and imaged using an Azure c600 Molecular Imager. ImageJ was used to align the bands, improve contrast (<20%), and normalize and quantify all bands.

2.8. LonP1 Protease Activity Assay

The total proteolytic activity of purified recombinant LonP1 (Abcam, ab160451) was analyzed using a Pierce Fluorescent Protease Assay Kit (Thermo Scientific™, 23266). A mixture of 200 nM LonP1 and 10 mM $MgCl_2$ was prepared in BupH™ Tris-buffered saline. LonP1 inhibitors or vehicle (DMSO) were then added, and the samples were incubated at 37°C for 1 h. Following this incubation, an equal volume of 0.04 mg/mL FITC-casein (Thermo Scientific™, 23267), 4 mM ATP (Thermo Fisher, R0441), and 10 mM $MgCl_2$ was added prior to measurement using a Biotek Synergy HT plate reader. Digestion of fluorescein-labeled casein was assessed by measuring fluorescence with excitation and emission filters at 490 and 525 nm, respectively.

2.9. Proteasome Activity Assay

Proteolytic activity was assessed using a Proteasome-Glo™ assay system (Promega, G8531), comprising Proteasome-Glo™ Chymotrypsin-Like Assay (G8621), Proteasome-Glo™ Trypsin-Like Assay (G8621) and Proteasome-Glo™ Caspase-Like Assay (G8621). The assay was performed according to the manufacturer's instructions. Tissue samples were flash frozen and ground using a Dounce Homogenizer (Fisher, 50-194-5205). Samples were then harvested in ice-cold lysis buffer composed of 50 mM HEPES (pH 7.4), 250 mM sucrose, 5 mM $MgCl_2$, 0.5 mM DTT, and 40 mM KCl in deionized, sterile water. For D-54 MG, cells were seeded at a density of 200,000 cells per well onto a 6-well plate and subsequently exposed to LonP1 inhibitors (BT317, BT395, BT397, and BT399) at the specified concentrations and endpoints. The lysates were incubated on ice for 30 min and centrifuged at 14,000 rpm for 10 min at 4°C. The supernatants were collected and mixed 1:1 with stabilizing buffer composed of 40 mM HEPES (pH 8.0), 1 mM EDTA, and 20%

glycerol in deionized, sterile water. The protein concentration was standardized using the DC Protein Assay (Bio-Rad, 500-0114) with a SpectraMax Plus 384 microplate reader. Samples were then diluted with ice-cold proteasome dilution buffer and plated in a black, clear, flat-bottom 96-well plate at a concentration of 8 µg protein in 50 µL/well (n = 3-4 replicates/sample). The plates were placed on a plate shaker at 300-500 rpm for 30 s, followed by incubation for 10-30 minutes incubation at room temperature. Luminescence was read using a Biotek Synergy HT plate reader.

2.10. BT317 and TMZ Administration and Maximum Tolerated Dose (MTD) Escalation

BT317 and TMZ was reconstituted in DMSO to create a concentrated stock prior to further dilution in 500 µL 1XPBS to generate the correct dosage for intraperitoneal injection (i.p.) in 10-14 week-old Rag1 KO immunodeficient mice (Jackson Laboratory, B6.129S7-*Rag1*^{tm1Mom}/J). Mice were monitored following injection and the clinical score was determined based on activity, appearance, and body condition with a maximum score of 3, which is necessary to define the MTD[36]. Mass spectrometry was performed on flash-frozen brains and tail vein blood draws by contract research organizations (Cyprotex and Biotechnology Innovation and Optimization Center) to determine BT317 levels.

2.11. Patient-derived Orthotopic Xenograft Model

The patient-derived lines DB70, DB76, DB77 and 83MES were seeded into 3-dimensional organoids using an established methodology[37]. Upon full expansion, the organoids were dissociated, and 1,000-10,000 cells were intracranially implanted into the right frontal lobe of 10-14 week-old Rag1 KO immunodeficient mice (Jackson Laboratory, B6.129S7-*Rag1*^{tm1Mom}/J). After 5 or 10 days, treatment was initiated as specified, with intraperitoneal (i.p.) injections every other day for a total of 5 doses over a span of 5 or 10 days as specified. Animals were observed daily and sacrificed upon observation of distress, including hemiparesis, obtundation, hunchback, or weight loss of 20% from the maximum weight achieved.

2.12. Quantitative Polymerase Chain Reaction Assay

For each cell line, growth conditions were standardized and ~500,000 cells were collected and flash frozen. Samples were then processed according to the Quick-RNA™ Miniprep Plus Kit (Zymo Research, R1057) specifications to prepare pure RNA samples. These were used to generate cDNA samples using a two step reverse transcriptase and polymerase chain reaction with PerfeCTa SYBR Green Supermix and transcript appropriate primers. The primers used include: LONP1 (5'- ATGGAGGACGTCAAGAAACG-3', 5'-GACGCTGAAGCGGAAGTACTC-3') and B-Actin Primer Set (Qiagen, QT00095431). After preparing master mixes samples were prepared in quadruplicate in a 96-well Reaction Microplates (Fisher Scientific, 4346907) and measured following a standard qtPCR protocol with a QuantStudio 7 Real-Time PCR System. Annealing temperature and length was optimized for each primer pair. Amplification was measured as fluorescence in quadruplicate replicates and analyzed using QuantStudio 7 software.

2.13. Statistical Analysis

Data were analyzed using Student's *t*-test or log-rank (Mantel-Cox) test when appropriate. Data are presented as mean ± standard error of the mean (SEM). Significance between groups is denoted by **P* <0.05, ***P* <0.01, ****P* < 0.001. Data were analyzed using the GraphPad Prism 5.0 software (GraphPad Software, La Jolla, CA, USA). For the XTT viability assays, raw data were processed using a log transform and a dose-response inhibition nonlinear model to determine IC50 and standard error. The statistical significance of the Kaplan-Meier survival curve was verified using the Mantel-Cox log-rank test.

Results

3.1 Dual LonP1 and Chymotrypsin-like Activity Exhibits Enhanced Synergy on IDH1 Mutant Malignant Astrocytoma Patient Derived Lines and Induces Greater Autophagy as Compared with IDH Wildtype Lines.

Previous findings suggested that dual LonP1 and chymotrypsin-like (CT-L) proteasome inhibition may be an effective strategy for targeting cancer cells; however, the exact mechanism has not been validated. Here, we demonstrated that the selective LonP1 inhibitor, CDDO-ME[28], and CT-L proteasome inhibitor, Carfilzomib (CFZ)[28,29], have strong synergy in reducing viability of multiple patient-derived malignant astrocytoma lines (**Fig. 1A**). Interestingly, the IDH1-mutant astrocytoma patient-derived lines DB70 and DB76 are sensitive to CDDO-ME doses as low as 200 nM CDDO-ME with CFZ at 1 and 5 nM; however, this combination has more limited activity against IDH wildtype DB77 and 83MES lines (e.g., >400 nM CDDO-ME, **Fig. 1B**). In the DB70 line, CDDO-ME treatment (200 nM) increased levels of the autophagy marker, LC3B-I[38] , which is further increased by 3, 8, 1.5-fold with co-incubation of 5 nM CFZ at 1, 12 and 24 h, respectively. In DB76, a 13, 1.5, 3-fold increase was observed in LC3B-I at 1, 12 and 24 h, respectively. CFZ alone did not alter LC3B-I levels (**Fig. 1C**). Furthermore, a significant increase in reactive oxygen species (by ~50%) is observed after 12 h of 200 nM CDDO-ME and 5 nM CFZ treatment (**Fig. 1D**) as opposed to either CFZ or CDDO-ME separately. However, none of the aforementioned treatments resulted in an increase in ROS in the 83MES line.

3.2. Structure Activity Relationship Modeling for Developing CC4 Derivatives.

Our previous work with CC4 demonstrated that LonP1 inhibition could inhibit astrocytoma cell growth, adaptation to hypoxic conditions, and increase the anti-tumor efficacy of TMZ[22]. Coumarinic compounds have been found to exhibit high hepatotoxicity[39]. To decrease off-target toxicity and improve anti-tumor efficacy, we derived four novel LonP1 inhibitors from CC4 using structure-activity relationship (SAR) modeling. A library of small molecules (e.g., BT395, BT397, BT399, and BT317) was identified *in silico,* using customized computational protein structure modeling programs M4T, MMM, Mutate, and SAR with Autodock4, Surflex-Dock, ICM, PESD, and SFC (B. Das, unpublished data). The CC4 ester group was modified to develop peptidomimetic compounds (amides and oxadiazoles) with increased water solubility. As a part of our rational design study, rings **A**, **B** and **C** were modified (**Fig. 2A**). Finally, the hydrophobic portion of rings **A** and **B** was replaced with quinolinolin-2 (1H)-1 to improve solubility (**Fig. 2B**; BT317). We developed also developed a library of additional CC4 derivatives; as shown in **Supplementary Fig. 2**. In Ring **A**, the benzyl group is prone to oxidation *in vivo* by oxidative cytochrome enzymes to form acidic chloride, which is associated with high toxicity. Therefore, chlorine was directly substituted at position 6 of the ring. The hydroxyl group on ring **C** was converted to a boronic ester group. The boronic acid and potassium salts of trifluoroborate and acid isosteres are known to increase cell permeability and reduce toxicity[40]. Furthermore, boronic acid and ester-based prodrugs were used as templates for ring **C** because boronic acid is selective for H_2O_2[31].

3.3. Novel CC4 Derivative, BT317, Exhibits On-Target Inhibition of LonP1 Protease and Proteasome Activity

Using our structure-activity relationship modeling approach, we derived BT317, BT395, BT397 and BT399 from CC4 and evaluated their relative LonP1 and proteasome inhibition profiles. To evaluate the on-target inhibition potency of these compounds, we assessed LonP1 protease activity inhibition using a FITC-casein assay (**Fig. 3A and Supplementary Fig. 3A**). BT317 demonstrated LonP1 protease inhibition with an IC_{50}=56 µM, while BT397 exhibited similar inhibition with an IC_{50}=58 µM. The other inhibitors showed no inhibition of LonP1 protease activity (data not shown). Since most LonP1 inhibitors exhibit dual inhibition of LonP1 and proteasome[23], we next examined whether the compounds also inhibit the 20S proteasome. For this assay, we prepared extracts from the established malignant glioma cell line, D-54 MG (**Fig. 3B**). At 10 µM, BT317 yielded a ~98 and 96% reduction in CT-L activity, a ~26% and 27% reduction in trypsin-like (T-L) activity, and a ~23% and 30% reduction in caspase-like (C-L) activity at both 1 and 4 h, respectively. The proteasomal activity of all three complexes returned to baseline at 8 h post-treatment. The BT395, BT397 and BT399 compounds showed limited inhibition of proteasome activity (**Supplementary Fig. 3C**). The antioxidant N-acetyl cysteine (NAC) inhibits the production of ROS and is a known blocker of proteasome inhibitors[41]. BT317 proteasome inhibition was eliminated by 10 mM NAC co-treatment.

In contrast to the other tested compounds, BT317 demonstrated quicker kinetic inhibition of CT-L proteasome activity than BTZ (**Fig. 3B**), which is a potent dual LonP1 and CT-L proteasome inhibitor approved for the treatment of multiple myeloma[42]. The observed CT-L inhibition by BTZ demonstrates limited inhibition by comparison to BT317. Given the potent on-target LonP1 protease inhibition of BT317 and its accelerated CT-L proteasome inhibition, we selected BT317 for further evaluation as a dual LonP1/proteasome targeted therapy in our astrocytoma models.

The mitochondrial matrix protein aconitase (Aco2) is the most important protease substrate for LonP1[43]. To evaluate the effect of BT317 on LonP1 substrate levels, we treated the established IDH wildtype D-54 MG and U-87 MG glioma lines with 10 µM BT317, well below the expected LonP1 protease inhibition concentration, IC_{50} = 56.03 µM (**Fig. 3C**). The D-54 MG line responded with a pronounced Aco2 protein level increase of 2-fold at 1 h; however, this was quickly reversed by 8 and 24 h. TFAM was still elevated by 3-fold at 24 h. We also compared this result with 100 nM Bortezomib (BTZ), a dual LonP1[30] and CT-L proteasome inhibitor. In the D-54 MG line, BTZ resulted in decreases in Aco2 levels at 24 h to 0.3-fold; however, it increased TFAM levels by 4-fold. In the U-87 line, BT317 resulted in the accumulation of Aco2 gradually to 3-fold and TFAM accumulated by 1.5-fold after 24 h and this effect was similarly mimicked by BTZ with 2.4 and 2.1-fold increase in protein levels, respectively. The LonP1 substrate accumulation/degradation observed exceeded what was expected given that previously demonstrated LonP1 protease inhibition.

3.4. BT317 Exhibits Synergy with Temozolomide in Autophagy-Dependent Cell Death in IDH1 Mutant Malignant Astrocytoma

Current glioma research and clinical trials emphasize the role of GSCs in tumor maintenance, resistance to therapies, and local invasion[44]. The patient-derived lines are enriched for tumor-initiating cancer stem cells by passaging in serum-free, suspension culture with referenced growth factors and have been shown to recapitulate the expression profile of the original patient sample[45]. Using the XTT assay, we determined

the IC_{50} viability of established and patient-derived GSC lines in response to 72 h of exposure to BT317 at graded doses (**Fig. 4A panel 1**). BT317 had increased toxicity towards the patient-derived GSC lines (i.e., 83MES, DB70, DB76, DB77, DB81; **Supplemental Table 1**) as compared to the established and differentiated astrocytoma lines, consistent with previous research which demonstrated that GSC are more sensitive to proteosome and LonP1 inhibition as compared with the more differentiated established lines[46]. The sensitivity of the DB70 line did not differ significantly from the DB81 line, derived from the same patient following recurrence. BT317 also showed less activity towards the CHLA-200 pediatric line (IC_{50}=73.61 µM). The normal cell lines, HPF242 and MCF10A, fibroblasts, and human astrocytes, also exhibited higher viability following treatment with BT317. Furthermore, BT317 synergized with 10 µM TMZ to decrease cell viability in the TMZ-resistant DB70 and DB76 GSC lines (recurrence following TMZ treatment) (**Fig. 4A panel 2, and S4A**). Interestingly, this synergy was not observed in the IDH wildtype lines, DB77 and 83MES (**Fig. 4A panel 3 and S4A**). Co-incubation of 10 µM BT317 with 10 µM TMZ in the DB70 line resulted in a significant increase in ROS by 1.5-fold (**Fig. 4B**). BT317 alone did induce a significant increase in ROS by 1.3-fold at 8 h in the DB70 line; however, only a slight decrease in ROS to 0.78-fold was observed at 4 h following treatment in the 83MES line (**Supplementary Fig. 4C**). The IDH1 mutant lines exhibited increased LC3B-I and II at 1, 12, 24 h post-treatment and this was reversed with co-incubation with 10 µM TMZ. Furthermore, C-MET and FOXM1 levels increased with BT317 or TMZ alone; however, the combination resulted in a decrease in C-MET and FOXM1 levels. This also coincided with a significant increase in Aco2 and TFAM with or without TMZ. The mTOR pathway (e.g., pAKT), which is capable of suppressing autophagy, was also upregulated with TMZ incubation at the earlier timepoints in the DB70 line; however, this was less obvious in the DB76 line, where there was a change of 0.57 and 1.83-fold for both bands at 1 h after combinatorial treatment (**Fig. 4C**). In the IDH1 wildtype lines, BT317 also increased LC3B-I, Aco2 and TFAM levels. DB77 showed a spike in LC3B-I levels by 7.62-fold that was reduced to 1.74-fold by 24 h, and demonstrated partial ablation of autophagy induced by co-incubation with TMZ. The 83MES line did not show significant induction of autophagy; however, it demonstrated a 2-fold ablation following incubation with TMZ at 24 h. Both BT317 and TMZ resulted in an increase in pAKT levels. In contrast, the DB77 line did exhibit elevated pAKT at 1 h with co-treatment and 24 h with TMZ alone (**Fig. 4C and S4B**) The more modest increase in pAKT following TMZ treatment could be due in part to the increased resistance to TMZ alone exhibited by the DB76 and DB77 lines – particularly at 10µM TMZ. In the IDH mutant DB76 line, the large autophagic response with BT317 treatment may partly explain its sensitivity to modest activation of mTOR signaling with TMZ treatment (**Supplementary Fig. 4D**). This muted autophagic response highlights the limited autophagy-induced cell death at 25uM BT317 in the DB77 line and the lack of autophagy-dependent cell death in the 83MES line, following co-incubation with 3mM 3-methyladenine (3-MA), an autophagy inhibitor. As expected in the IDH1 mutant lines, autophagy-dependent cell death was evident at lower concentrations of BT317 (**Fig. 4D**). Furthermore, the combinatorial treatment resulted in overall reduction in levels of FOXM1 and most significantly by ~2-fold at the 24 h timepoint for DB70 and DB76. This mimics previous observations with the combinatorial treatment of BTZ and TMZ[33]. Both DB77 and 83MES showed a relative increase of ~0.2-fold at 24 h. It was previously reported that TMZ targets more differentiated populations with an average IC_{50} of ~540 µM against similar glioma lines[47], whereas BT317 offers far greater efficacy against the harder to eradicate GSC populations (**Supplementary Table 1**). Furthermore, the these data highlight the potential use of BT317 in combination with TMZ as a treatment modality to target diverse cell populations and potentially to reverse malignant astrocytoma treatment resistance.

3.5. BT317 Exhibits Low Toxicity and its Activity is Localized to the Tumor Microenvironment

Previous development of proteasome inhibitors for the treatment of GBM was limited by either poor BBB penetrance (i.e., BTZ)[31] or by the presence of the central nervous system (i.e., MRZ= marizomib, confusion, ataxia)[48] or peripheral nervous system (BTZ, peripheral neuropathy)[49] toxicity. The development of these toxicities is directly related to the level of proteasome inhibition in the blood and in the normal brain[50].

Prior to evaluating efficacy, we established the maximum tolerated dose (MTD). Using a previously established methodology[36], we observed the clinical score following treatment (n=2) with iterative 50% dose escalation until we determined the MTD to be >180 mg/kg (data not shown). We repeated a continuous dose series over 10 days with 100 mg/kg of BT317 every other day or daily. There was no noticeable drop in weight or any observable clinical signs (**Fig. 5A**). Next, we administered 100 mg/kg BT317 and 25 mg/kg TMZ or 100 mg/kg BT317 and 50 mg/kg TMZ daily for 10 days. A temporary drop in weight and minor clinical signs were observed following the first 2 doses with 100 mg/kg BT317 and 50 mg/kg TMZ; however, the animal weight normalized by day 4 and no further clinical signs were observed. Novel therapeutic candidates for malignant astrocytomas must have superior BBB penetrance, target GSCs, synergize with the standard of care, TMZ, and demonstrate improved survival *in vivo*. To assess BBB penetrance, 9x BALB/c mice received a single intraperitoneal (i.p.) injection of BT317 (3 mg/kg). The animals were euthanized 30, 60, and 120 min post-BT317 injection (n=3 per endpoint). Brain and plasma samples were collected, and BT317 (ng/mL) levels were quantified using mass spectrometry (**Fig. S5A**). BT317 levels reached ~390 ng/mL in the brain at 30 min and decreased to ~55 ng/mL at 120 min post-injection. At all measured endpoints, levels in the brain were significantly higher than those in the plasma.

To evaluate the on-site activity of BT317, we performed an intracranial implantation with the DB70 line and after 15 days administered a single dose of 100 mg/kg of BT317 to the mice prior to analyzing proteasome activity in the blood, healthy brain, and intracranial tumor mass (**Fig. 5B**). The animals were euthanized 1 and 4 h post-injection (n=6 per endpoint). BT317 showed ~70% and 60% inhibition of CT-L and C-L activity in the tumor, respectively, compared with ~50% and 25% for MRZ at 4 h. Only MRZ showed CT-L inhibition in the normal healthy brain with a ~40% reduction at 1-4 h. Furthermore, MRZ also inhibited CT-L, T-L, and C-L in the blood by ~90%, 35-45%, and 30%, respectively. BT317 did not inhibit proteasome activity in the blood. Both BT317 and MRZ showed accumulation of Aco2 in the tumor at 4 h with ~60-70% increase on average (**Supplementary Fig. 4**).

3.6. BT317 and Combinatorial Treatment with BT317 and TMZ Increases Survival

Next, we assessed the efficacy in an orthotopic xenograft model using the GSC patient-derived, IDH1-R132H DB70 and DB76 lines. Rag1 KO mice were intracranially implanted with DB70 or DB76 (1000 cells/mouse), dissociated from a novel *in vitro,* organoid model[37] (**Fig. 6**). A total of 5 doses were administered at 100 mg/kg BT317 ± 50 mg/kg TMZ daily, starting 10 days after intracranial xenograft implantation and continuing for a total of 5 days. BT317 alone significantly improved the median survival by 1 ($p<0.05$) and 3 days ($p<0.05$) in the DB70 and DB76 xenografts, respectively. The combination of BT317 and TMZ significantly improved overall survival ($p<0.01$); however, median survival for the combinatorial cohorts could not be determined by the end of the experiment. We also found that earlier dosing regimen starting on day 5 for a total 5 doses of 100 mg/kg BT317 every other day significantly increased median survival from 25 to 33 days in the DB70 PDX model (10,000 cells/mouse, **Supplementary**

Fig. 6A). The 83MES PDX model also showed a modest increase in median overall survival from 17.5 to 19 days; however, this required an escalated dosage of 150 mg/kg BT317 (10,000 cells/mouse, **Supplementary Fig. 6B**).

Discussion and Conclusion

Previously, we demonstrated that the LonP1 inhibitor, CC4, was effective against established glioma lines and that proteosome inhibition with marizomib is effective in *in vitro* and *in vivo* glioma models, though its clinical use is limited by significant CNS toxicity[51]. Here we have reported on the designing of the novel LonP1 and CT-L proteosome inhibitor, BT317, which has specific activity and limited toxicity.

For our rational design and SAR modeling, we used customized computational protein structure modeling programs, as well as standard programs, to identify the lead compounds that could be derived from CC4 to improve solubility and BBB permeability and reduce toxicity. For compound design, we used the Lipinski rule of 5 with the following considerations: (1) biological activity (i.e., more sp3 carbon atoms), (2) ease of synthesis, and (3) moderate compound complexity to minimize toxicity and off-target effects[52].

Our lead molecule, BT317, exhibited dual inhibition of LonP1 protease activity and CT-L proteasomal activity, on-target LonP1 inhibition, BBB permeability, low animal toxicity, and prolonged survival with and without the standard-of-care in two patient-derived IDH1-R132H GSC intracranial xenograft models. BT317 accumulated at higher levels in the brain than in the plasma at 30 min post-administration. Its potent dual inhibitory activity can be compared with that of BTZ, a potent proteasome inhibitor that also inhibits LonP1 protease activity. However, BTZ has limited penetrance into the brain, and a phase II clinical trial of BTZ and bevacizumab in recurrent GBM was hindered due to dose-limiting sensory neuropathy associated with BTZ[53]. Another CT-L proteasome inhibitor tested for GBM was ritonavir. Nonetheless, ritonavir failed to demonstrate efficacy due to the development of resistance, *in vivo*[54]. Marizomib has also shown improved survival in orthotopic GBM models; however, it has exhibited underlying issues with significant CNS toxicity (confusion, ataxia, fatigue)[55] in phase 2 studies and did not improve survival in a phase 3 randomized clinical trial[48]. This toxicity is represented by the high rate of marizomib-treated patients that have neurologic (67%) and psychiatric (52%) adverse events[51]. Additionally, the high MTD and specific tumor activity of BT317 further demonstrate its potential as a less toxic dual LonP1 and proteasomal inhibitor for GBM treatment.

GBM is characterized by mitochondrial dysfunction, including metabolic shifts towards aerobic glycolysis, elevated ROS generation, and sensitivity to metabolic stress[22]. Aconitase participates in the tricarboxylic acid cycle (TCA) by converting citrate to isocitrate; however, its involvement in malignant astrocytoma metabolism is unclear. Recent studies have shown that Aco2 levels are decreased in breast cancer cell lines and patient-derived tumor biopsies, and Aco2 overexpression impairs breast cancer cell proliferation and mitigates the Warburg effect by redirecting pyruvate to the mitochondria[56]. In addition to its role in the TCA cycle, aconitase also promotes mtDNA stability by interacting with nucleoids (protein-mtDNA complexes)[57]. Our findings revealed pronounced Aco2 accumulation in stable GBM lines and patient-derived GSCs following BT317 exposure. Notably, BT317 induced Aco2 accumulation at 10 µM despite the IC_{50}=56 µM for LonP1 protease inhibition. This accumulation was more pronounced than that induced by 100 nM BTZ, with previously reported LonP1 protease inhibition (IC_{50}=60 nM)[30]. BT317 also increased Aco2 levels in an intracranial xenograft model. Further investigation of the role of Aco2 in malignant

astrocytoma metabolism and how the different BT317 moieties may enhance LonP1 protease inhibition is warranted.

An important finding of our study is that the combination of BT317 and TMZ is more effective than BT317 or TMZ alone in IDH1-R132H GSC lines DB70 and DB76. The IDH wildtype GBM and astrocytoma cell lines and the normal human fibroblast cell lines, HPF242 and MCF-10A, were less sensitive to combinatorial treatment. Introduction of IDH1-R132H mutation to wildtype gliomas has been observed to increase ROS generation[58] and decrease HIF1A[59-61] and NRF2 signaling[62]; however, this may be due to an altered hypoxic response[63] and may also depend on the tumor microenvironment[59]. TMZ has been found to induce mTOR signaling (e.g., pAKT)[64,65] and also subsequently block autophagy[65] in the 12-60 h range. This inhibition of autophagy likely explains the strong synergy between TMZ and BT317, as BT317 clearly induces autophagy and blocking autophagy with 3-MA was found to induce cell death. Additionally, the maximum tolerated dose was exceptionally high, with little to no off-target proteasome inhibition. Targeting the GSC population is critical for overcoming glioma treatment resistance. The dependence of GSCs on LonP1 and CT-L proteasome activity is further highlighted by the upregulation of LonP1 in high-grade GSCs compared to low-grade GSCs and neural stem cells (**Supplementary Fig. 2**). Proteasome activity also plays a key role in cancer treatment resistance[25,26]. Interestingly, gliomas have elevated CT-L proteasome activity and, generally, an increase in this activity serves as a compensatory response to prooxidative treatment[66]. Additional studies are vital to further explore the role of LonP1 and CT-L proteasome activity in malignant glioma metabolism and whether dual inhibition could be useful for treating recurrent malignant astrocytoma based on patient-specific genetic determinants. Future work will also seek to understand the best route of administration, while also creating BT317 analogs that incorporate nanoparticles and other moieties to optimize on-site and on-target activity to further the development of new therapeutic options for malignant astrocytoma patients.

3. References

1. Ohgaki H, Dessen P, Jourde B, et al. Genetic Pathways to Glioblastoma: A Population-Based Study. *Cancer research.* 2004; 64(19):6892-6899.

2. Sathornsumetee S, Rich JN, Reardon DA. Diagnosis and Treatment of High-Grade Astrocytoma. *Neurologic Clinics.* 2007; 25(4):1111-1139.

3. Stupp R, Mason WP, van den Bent MJ, et al. Radiotherapy plus concomitant and adjuvant temozolomide for glioblastoma. *N Engl J Med.* 2005; 352(10):987-996.

4. Rominiyi O, Vanderlinden A, Clenton SJ, Bridgewater C, Al-Tamimi Y, Collis SJ. Tumour treating fields therapy for glioblastoma: current advances and future directions. *British Journal of Cancer.* 2021; 124(4):697-709.

5. Fisher JP, Adamson DC. Current FDA-Approved Therapies for High-Grade Malignant Gliomas. *Biomedicines.* 2021; 9(3).

6. Hegi ME, Diserens AC, Gorlia T, et al. MGMT gene silencing and benefit from temozolomide in glioblastoma. *N Engl J Med.* 2005; 352(10):997-1003.

7. Ohgaki H, Kleihues P. The definition of primary and secondary glioblastoma. *Clin Cancer Res.* 2013; 19(4):764-772.

8. Louis DN, Perry A, Wesseling P, et al. The 2021 WHO Classification of Tumors of the Central Nervous System: a summary. *Neuro-Oncology.* 2021; 23(8):1231-1251.

9. Yan H, Parsons DW, Jin G, et al. IDH1 and IDH2 mutations in gliomas. *N Engl J Med.* 2009; 360(8):765-773.

10. Golub D, Iyengar N, Dogra S, et al. Mutant Isocitrate Dehydrogenase Inhibitors as Targeted Cancer Therapeutics. *Front Oncol.* 2019; 9:417.

11. Liu Y, Lu Y, Celiku O, et al. Targeting IDH1-Mutated Malignancies with NRF2 Blockade. *J Natl Cancer Inst.* 2019; 111(10):1033-1041.

12. Li Z, Bao S, Wu Q, et al. Hypoxia-inducible factors regulate tumorigenic capacity of glioma stem cells. *Cancer Cell.* 2009; 15(6):501-513.

13. Gordan JD, Thompson CB, Simon MC. HIF and c-Myc: Sibling Rivals for Control of Cancer Cell Metabolism and Proliferation. *Cancer Cell.* 2007; 12(2):108-113.

14. Forsythe JA, Jiang BH, Iyer NV, et al. Activation of vascular endothelial growth factor gene transcription by hypoxia-inducible factor 1. *Molecular and Cellular Biology.* 1996; 16(9):4604-4613.

15. Kaur B, Khwaja FW, Severson EA, Matheny SL, Brat DJ, Van Meir EG. Hypoxia and the hypoxia-inducible-factor pathway in glioma growth and angiogenesis. *Neuro-oncology.* 2005; 7(2):134-153.

16. Yang L, Lin C, Wang L, Guo H, Wang X. Hypoxia and hypoxia-inducible factors in glioblastoma multiforme progression and therapeutic implications. *Experimental Cell Research.* 2012; 318(19):2417-2426.

17. Fukuda R, Zhang H, Kim JW, Shimoda L, Dang CV, Semenza GL. HIF-1 regulates cytochrome oxidase subunits to optimize efficiency of respiration in hypoxic cells. *Cell.* 2007; 129(1):111-122.

18. Rep M, van Dijl JM, Suda K, Schatz G, Grivell LA, Suzuki CK. Promotion of mitochondrial membrane complex assembly by a proteolytically inactive yeast Lon. *Science (New York, N.Y.).* 1996; 274(5284):103-106.

19. Liu T, Lu B, Lee I, Ondrovicova G, Kutejova E, Suzuki CK. DNA and RNA binding by the mitochondrial lon protease is regulated by nucleotide and protein substrate. *The Journal of biological chemistry.* 2004; 279(14):13902-13910.

20. Quiros PM, Espanol Y, Acin-Perez R, et al. ATP-dependent Lon protease controls tumor bioenergetics by reprogramming mitochondrial activity. *Cell Rep.* 2014; 8(2):542-556.

21. Cheng CW, Kuo CY, Fan CC, et al. Overexpression of Lon contributes to survival and aggressive phenotype of cancer cells through mitochondrial complex I-mediated generation of reactive oxygen species. *Cell Death Dis.* 2013; 4:e681.

22. Di K, Lomeli N, Wood SD, Vanderwal CD, Bota DA. Mitochondrial Lon is over-expressed in high-grade gliomas, and mediates hypoxic adaptation: potential role of Lon as a therapeutic target in glioma. *Oncotarget.* 2016; 7(47):77457-77467.

23. Bayot A, Basse N, Lee I, et al. Towards the control of intracellular protein turnover: Mitochondrial Lon protease inhibitors versus proteasome inhibitors. *Biochimie.* 2008; 90(2):260-269.

24. Stahlberg H, Kutejová E, Suda K, et al. Mitochondrial Lon of Saccharomyces cerevisiae is a ring-shaped protease with seven flexible subunits. *Proceedings of the National Academy of Sciences.* 1999; 96(12):6787-6790.

25. Adams J. The proteasome: structure, function, and role in the cell. *Cancer Treat Rev.* 2003; 29 Suppl 1:3-9.

26. Patel NM, Nozaki S, Shortle NH, et al. Paclitaxel sensitivity of breast cancer cells with constitutively active NF-kappaB is enhanced by IkappaBalpha super-repressor and parthenolide. *Oncogene.* 2000; 19(36):4159-4169.

27. Maneix L, Sweeney MA, Lee S, et al. The Mitochondrial Protease LonP1 Promotes Proteasome Inhibitor Resistance in Multiple Myeloma. *Cancers (Basel).* 2021; 13(4).

28. Lee J, Pandey AK, Venkatesh S, et al. Inhibition of mitochondrial LonP1 protease by allosteric blockade of ATP binding and hydrolysis via CDDO and its derivatives. *The Journal of biological chemistry.* 2022; 298(3):101719.

29. Gibellini L, Pinti M, Bartolomeo R, et al. Inhibition of Lon protease by triterpenoids alters mitochondria and is associated to cell death in human cancer cells. *Oncotarget.* 2015; 6(28):25466-25483.

30. Csizmadia V, Hales P, Tsu C, et al. Proteasome inhibitors bortezomib and carfilzomib used for the treatment of multiple myeloma do not inhibit the serine protease HtrA2/Omi. *Toxicol Res (Camb).* 2016; 5(6):1619-1628.

31. Takeshima K, Mizuno K, Nakahashi H, Aoki H, Kanekiyo Y. Ratiometric Sensing of Hydrogen Peroxide Utilizing Conformational Change in Fluorescent Boronic Acid Polymers. *Journal of Analytical Methods in Chemistry.* 2017; 2017:7829438.

32. Huehnchen P, Springer A, Kern J, et al. Bortezomib at therapeutic doses poorly passes the blood–brain barrier and does not impair cognition. *Brain Communications.* 2020; 2(1).

33. Tang JH, Yang L, Chen JX, et al. Bortezomib inhibits growth and sensitizes glioma to temozolomide (TMZ) via down-regulating the FOXM1-Survivin axis. *Cancer Commun (Lond).* 2019; 39(1):81.

34. Seidel S, Garvalov BK, Acker T. Isolation and Culture of Primary Glioblastoma Cells from Human Tumor Specimens. In: Rich IN, ed. *Stem Cell Protocols*. New York, NY: Springer New York; 2015:263-275.

35. Van der Borght K, Tourny A, Bagdziunas R, et al. BIGL: Biochemically Intuitive Generalized Loewe null model for prediction of the expected combined effect compatible with partial agonism and antagonism. *Sci Rep.* 2017; 7(1):17935.

36. Aston WJ, Hope DE, Nowak AK, Robinson BW, Lake RA, Lesterhuis WJ. A systematic investigation of the maximum tolerated dose of cytotoxic chemotherapy with and without supportive care in mice. *BMC cancer.* 2017; 17(1):684-684.

37. Hubert CG, Rivera M, Spangler LC, et al. A Three-Dimensional Organoid Culture System Derived from Human Glioblastomas Recapitulates the Hypoxic Gradients and Cancer Stem Cell Heterogeneity of Tumors Found In Vivo. *Cancer research.* 2016; 76(8):2465-2477.

38. Mizushima N, Yoshimori T. How to interpret LC3 immunoblotting. *Autophagy.* 2007; 3(6):542-545.

39. Vassallo JD, Hicks SM, Daston GP, Lehman-McKeeman LD. Metabolic Detoxification Determines Species Differences in Coumarin-Induced Hepatotoxicity. *Toxicological Sciences.* 2004; 80(2):249-257.

40. Lassalas P, Gay B, Lasfargeas C, et al. Structure Property Relationships of Carboxylic Acid Isosteres. *Journal of medicinal chemistry.* 2016; 59(7):3183-3203.

41. Halasi M, Wang M, Chavan Tanmay S, Gaponenko V, Hay N, Gartel Andrei L. ROS inhibitor N-acetyl-L-cysteine antagonizes the activity of proteasome inhibitors. *Biochemical Journal.* 2013; 454(2):201-208.

42. Manton CA, Johnson B, Singh M, Bailey CP, Bouchier-Hayes L, Chandra J. Induction of cell death by the novel proteasome inhibitor marizomib in glioblastoma in vitro and in vivo. *Scientific Reports.* 2016; 6(1):18953.

43. Bota DA, Davies KJ. Lon protease preferentially degrades oxidized mitochondrial aconitase by an ATP-stimulated mechanism. *Nature cell biology.* 2002; 4(9):674-680.

44. Chen J, Li Y, Yu T-S, et al. A restricted cell population propagates glioblastoma growth after chemotherapy. *Nature.* 2012; 488(7412):522-526.

45. Vik-Mo EO, Sandberg C, Olstorn H, et al. Brain tumor stem cells maintain overall phenotype and tumorigenicity after in vitro culturing in serum-free conditions. *Neuro Oncol.* 2010; 12(12):1220-1230.

46. Gong X, Schwartz PH, Linskey ME, Bota DA. Neural stem/progenitors and glioma stem-like cells have differential sensitivity to chemotherapy. *Neurology.* 2011; 76(13):1126-1134.

47. Ferretti M, Fabbiano C, Di Bari M, et al. M2 receptor activation inhibits cell cycle progression and survival in human glioblastoma cells. *Journal of cellular and molecular medicine.* 2013; 17.

48. Di K, Lloyd GK, Abraham V, et al. Marizomib activity as a single agent in malignant gliomas: ability to cross the blood-brain barrier. *Neuro-oncology.* 2016; 18(6):840-848.

49. Rutkowski S, Gerber NU, von Hoff K, et al. Treatment of early childhood medulloblastoma by postoperative chemotherapy and deferred radiotherapy. *Neuro-Oncology.* 2009; 11(2):201-210.

50. Velasco R, Alberti P, Bruna J, Psimaras D, Argyriou AA. Bortezomib and other proteosome inhibitors—induced peripheral neurotoxicity: From pathogenesis to treatment. *Journal of the Peripheral Nervous System.* 2019; 24(S2):S52-S62.

51. Roth P, Gorlia T, Reijneveld JC, et al. EORTC 1709/CCTG CE.8: A phase III trial of marizomib in combination with temozolomide-based radiochemotherapy versus temozolomide-based radiochemotherapy alone in patients with newly diagnosed glioblastoma. Paper presented at: ASCO Annual Meeting2021.

52. Lovering F, Bikker J, Humblet C. Escape from flatland: increasing saturation as an approach to improving clinical success. *Journal of medicinal chemistry.* 2009; 52(21):6752-6756.

53. Bota DA, Eroglu Z, Reardon DA, et al. Phase II clinical trial of bortezomib and bevacizumab combination in recurrent glioblastoma. *Journal of Clinical Oncology.* 2011; 29(15_suppl):2056-2056.

54. Laurent N, de Boüard S, Guillamo JS, et al. Effects of the proteasome inhibitor ritonavir on glioma growth in vitro and in vivo. *Mol Cancer Ther.* 2004; 3(2):129-136.

55. Bota DA, Mason W, Kesari S, et al. Marizomib alone or in combination with bevacizumab in patients with recurrent glioblastoma: Phase I/II clinical trial data. *Neurooncol Adv.* 2021; 3(1):vdab142-vdab142.

56. Ciccarone F, Di Leo L, Lazzarino G, et al. Aconitase 2 inhibits the proliferation of MCF-7 cells promoting mitochondrial oxidative metabolism and ROS/FoxO1-mediated autophagic response. *British Journal of Cancer.* 2020; 122(2):182-193.

57. Farooq MA, Pracheil TM, Dong Z, Xiao F, Liu Z. Mitochondrial DNA Instability in Cells Lacking Aconitase Correlates with Iron Citrate Toxicity. *Oxidative Medicine and Cellular Longevity.* 2013; 2013:493536.

58. Li LC, Zhang M, Feng YK, Wang XJ. IDH1-R132H Suppresses Glioblastoma Malignancy through FAT1-ROS-HIF-1α Signaling. *Neurol India.* 2020; 68(5):1050-1058.

59. Williams SC, Karajannis MA, Chiriboga L, Golfinos JG, von Deimling A, Zagzag D. R132H-mutation of isocitrate dehydrogenase-1 is not sufficient for HIF-1α upregulation in adult glioma. *Acta Neuropathol.* 2011; 121(2):279-281.

60. Yao J, Chakhoyan A, Nathanson DA, et al. Metabolic characterization of human IDH mutant and wild type gliomas using simultaneous pH- and oxygen-sensitive molecular MRI. *Neuro-Oncology.* 2019; 21(9):1184-1196.

61. Xu W, Yang H, Liu Y, et al. Oncometabolite 2-Hydroxyglutarate Is a Competitive Inhibitor of α-Ketoglutarate-Dependent Dioxygenases. *Cancer Cell.* 2011; 19(1):17-30.

62. Li K, Ouyang L, He M, et al. IDH1 R132H mutation regulates glioma chemosensitivity through Nrf2 pathway. *Oncotarget.* 2017; 8(17):28865-28879.

63. Dao Trong P, Rösch S, Mairbäurl H, et al. Identification of a Prognostic Hypoxia-Associated Gene Set in IDH-Mutant Glioma. *Int J Mol Sci.* 2018; 19(10).

694 **64.** Murphy SF, Varghese RT, Lamouille S, et al. Connexin 43 Inhibition Sensitizes Chemoresistant
695 Glioblastoma Cells to Temozolomide. *Cancer research.* 2016; 76(1):139-149.
696 **65.** Yu Z, Zhao G, Xie G, et al. Metformin and temozolomide act synergistically to inhibit growth of
697 glioma cells and glioma stem cells in vitro and in vivo. *Oncotarget.* 2015; 6(32):32930-32943.
698 **66.** Kretz-Remy C, Arrigo A-P. Modulation of the chymotrypsin-like activity of the 20S proteasome
699 by intracellular redox status: effects of glutathione peroxidase-1 overexpression and antioxidant
700 drugs. *Biol Chem.* 2003; 384(4):589-595.

701

702

703

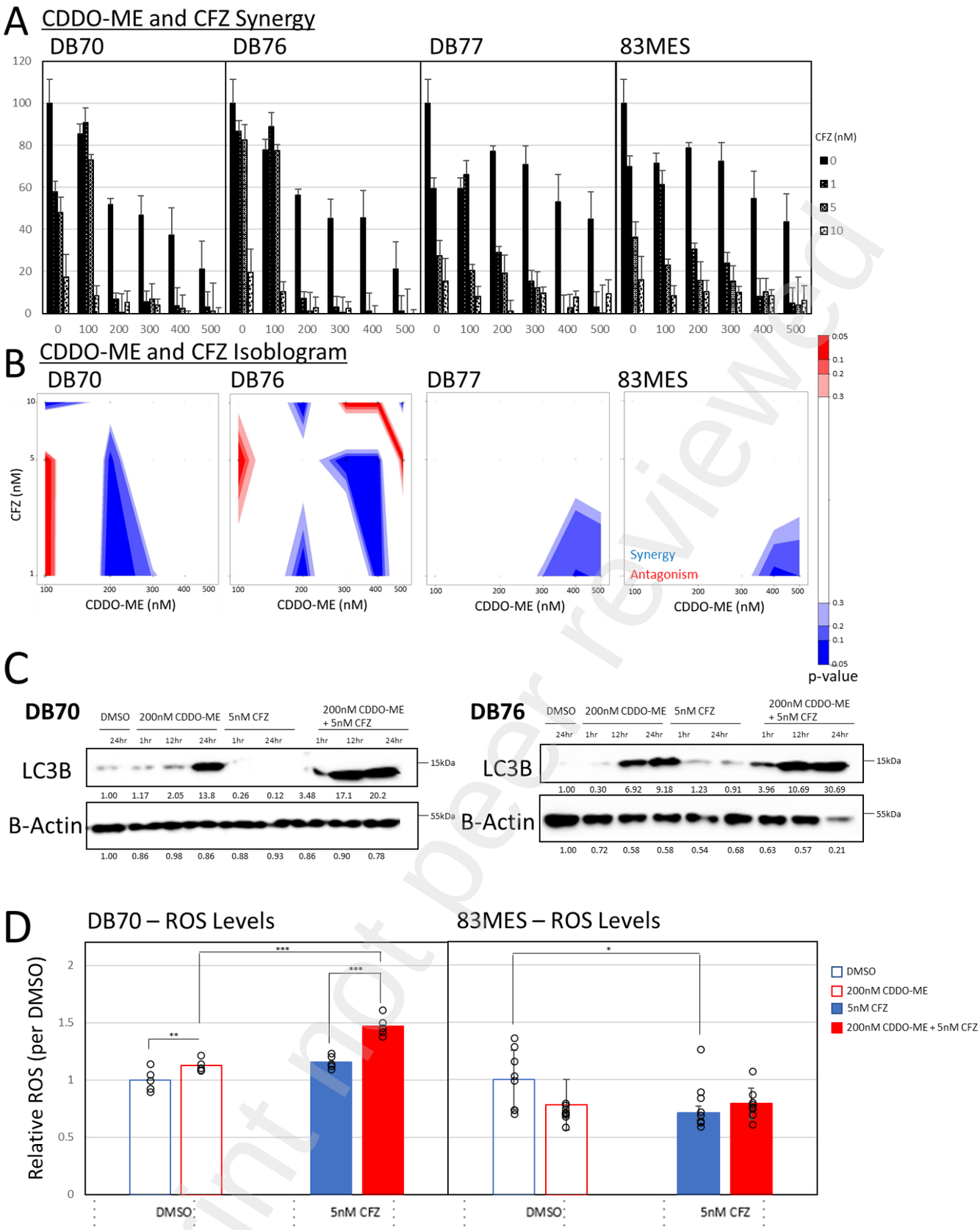

Figure 1. Dual LonP1 and Chymotrypsin-like Proteasome Inhibition has Greater Synergy in IDH1 Mutant Astrocytoma and Enhances Autophagy and ROS Production. (**A**) In combination with Carfilzomib, a selective chymotrypsin-like proteasome inhibitor, CDDO-ME, a known LonP1 inhibitor, demonstrates strong synergy at 200nM in IDH1 mutant lines, whereas (B) the IDH1 wildtype lines only show limited synergy at 400-500nM. (C) LC3B levels and (D) ROS levels were assessed following treatment with 5nM CFZ and/or 200nM CDDO-ME at 1, 12 and 24 h timepoints in DB70 and DB76. (E) Similarly ROS levels were analyzed in 83MES. Statistical significance was determined by t-test. * *P* <0.05, ***P* <0.01, ****P* <0.001; n.s., not significant.

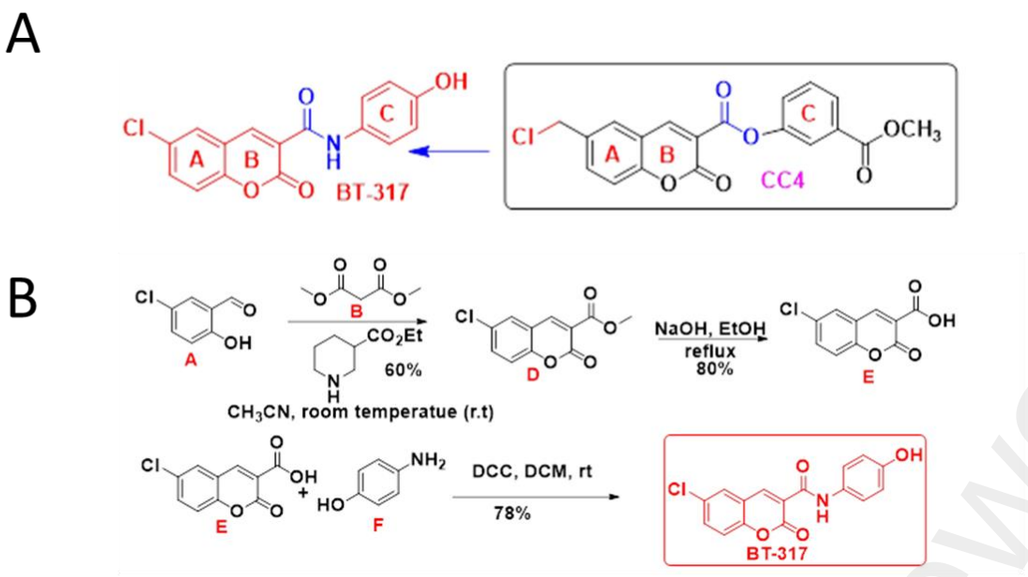

Figure 2. LonP1 small molecule inhibitor BT317 was derived from CC4. (**A**) BT317 is an analog of CC4. (**B**) Synthesis of BT317.

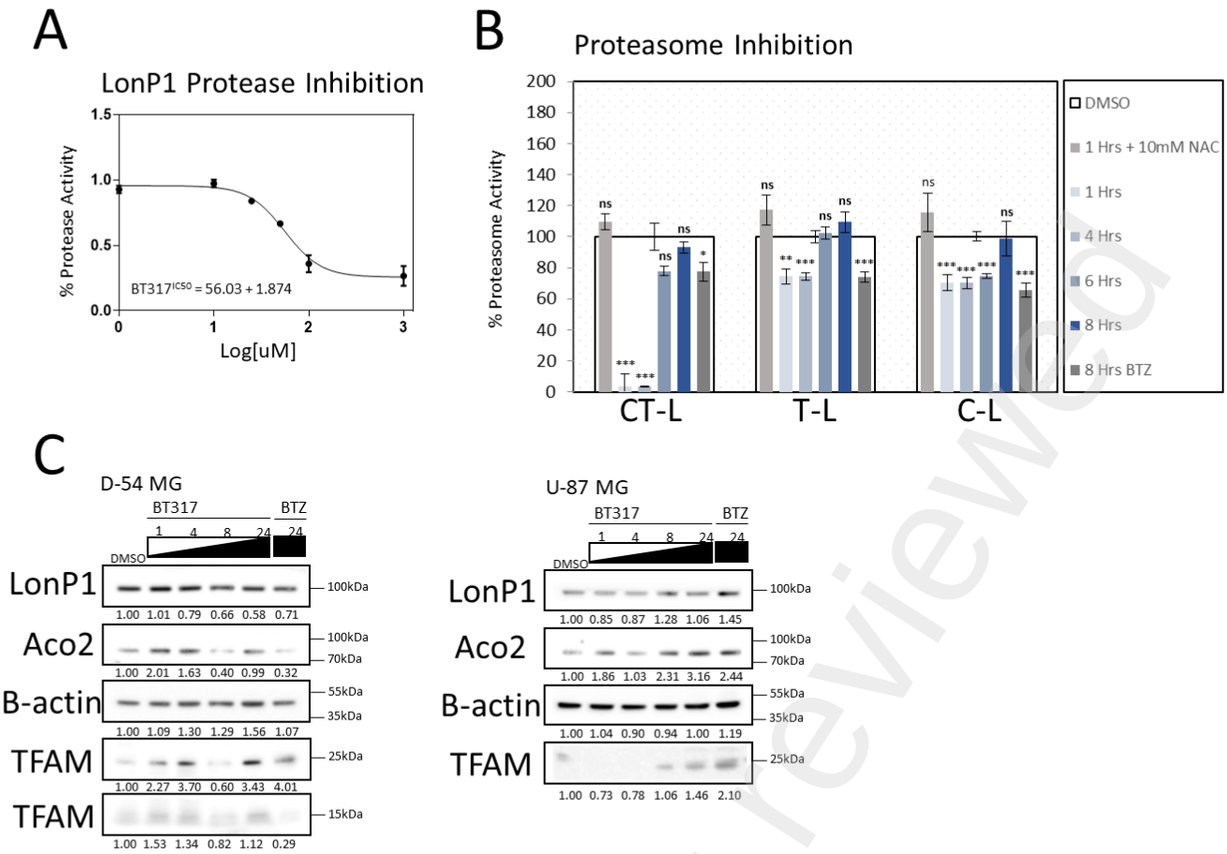

Figure 3. BT317 acts as a dual LonP1 and chymotrypsin-like proteasome inhibitor. (**A**) BT317 inhibition of LonP1 protease activity was assessed using a FITC-Casein substrate. (**B**) 10μM BT317 or 100nM BTZ were evaluated for proteasome inhibition at 1, 4, 6, 8 h. NAC was used to ablate proteasome inhibition. (**C**) The IDH1 wildtype U-251 and U-87 MG lines were treated with 10μM BT317 and demonstrated increased Aco2 and TFAM levels. Data are presented as mean ± SEM of at least 3 replicates. Statistical significance was determined by t-test. * *P* <0.05, ** *P* <0.01, *** *P* <0.001; n.s., not significant.

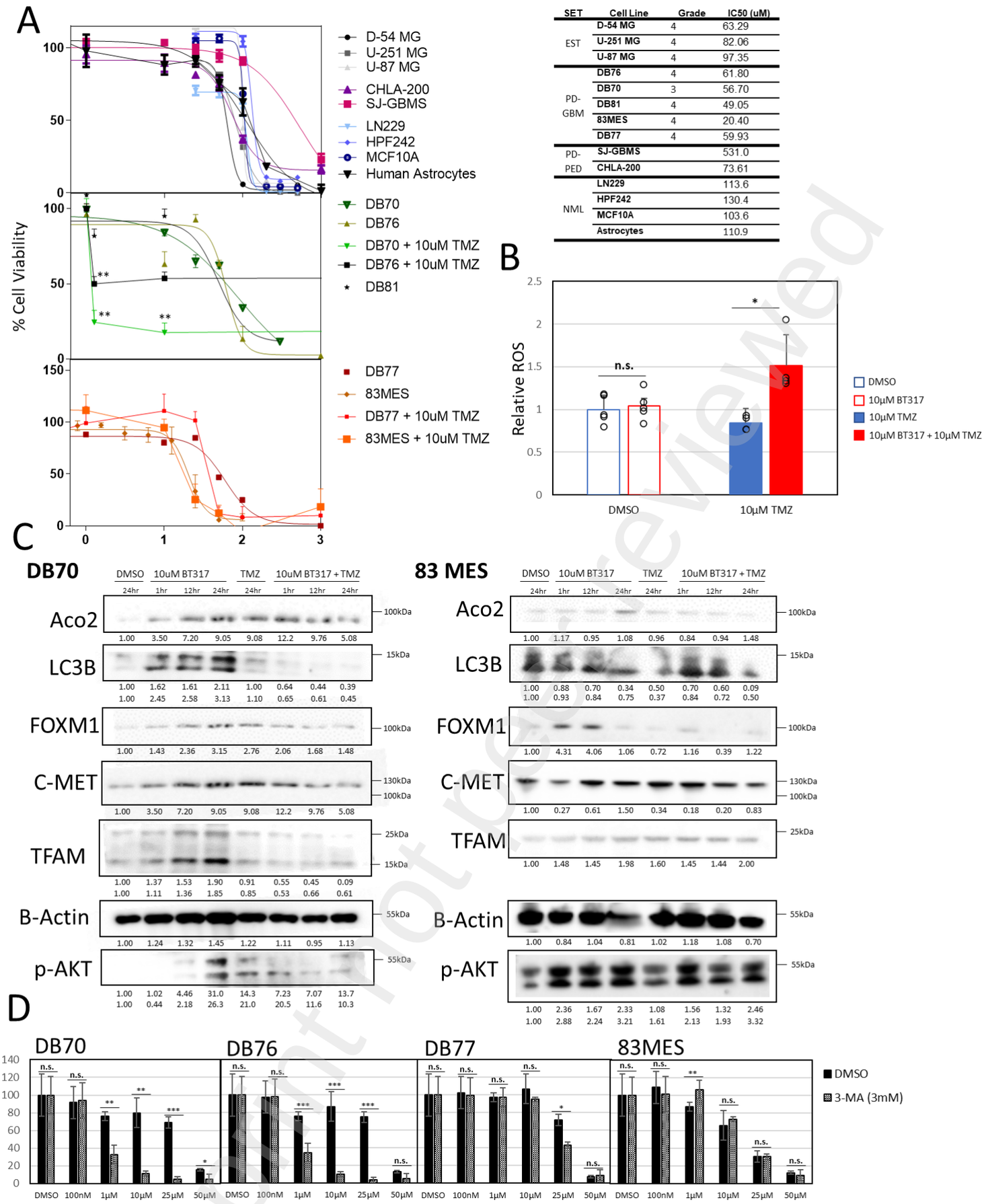

SET	Cell Line	Grade	IC50 (uM)
EST	D-54 MG	4	63.29
	U-251 MG	4	82.06
	U-87 MG	4	97.35
PD-GBM	DB76	4	61.80
	DB70	3	56.70
	DB81	4	49.05
	83MES	4	20.40
	DB77	4	59.93
PD-PED	SJ-GBMS		531.0
	CHLA-200		73.61
NML	LN229		113.6
	HPF242		130.4
	MCF10A		103.6
	Astrocytes		110.9

Figure 4. BT317 drives autophagy-dependent cell death in specifically IDH1 mutant astrocytoma and TMZ works synergistically by blocking autophagy. (A) Astrocytes, multiple fibroblast lines, established GBM lines (panel 1), IDH1 mutant glioma lines DB70 and DB76 ± 10μM TMZ (panel 2), and IDH1 wildtype glioma lines DB77 and 83MES ± 10μM TMZ (panel 3) were treated with titrated doses of BT317 for 5 days prior to measuring viability. (B) ROS were measured using CellROX Orange at 12 h and (C) protein samples analyzed following incubation with 10μM BT317 ± 10μM TMZ at 1, 12 and 24 h as detailed. (D) The IDH1 mutant and wildtype lines were analyzed for autophagy-dependent cell death following treatment with a titer of BT317 and co-incubation with 3mM 3-MA for 5 days. Statistical significance was determined by t-test. * *P* <0.05, ***P* <0.01, ****P* <0.001; n.s., not significant.

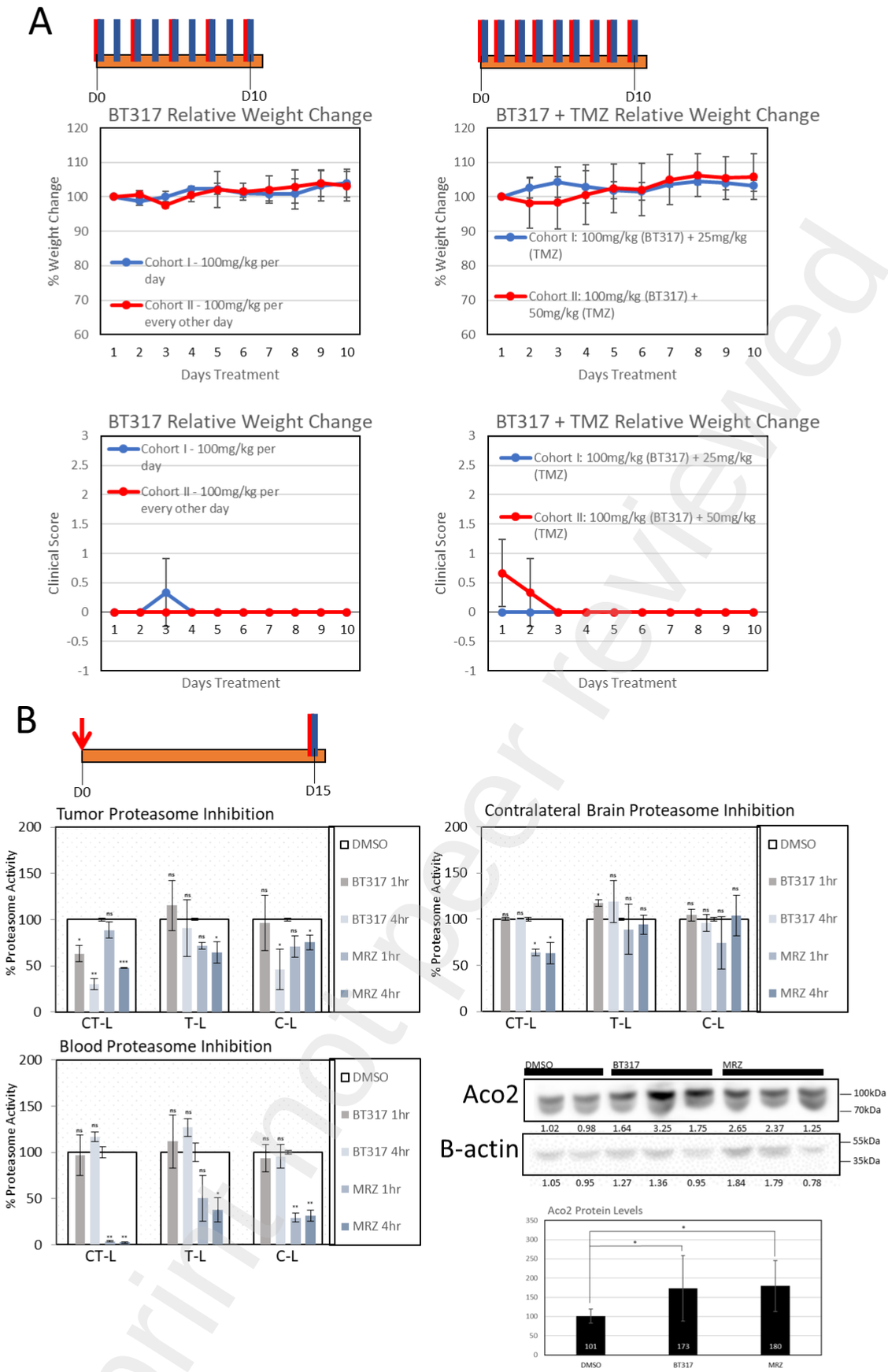

Figure 5. The combination of BT317 and TMZ has minimal toxicity in NSG mice. (**A**) BT317 was administered at 100mg/kg every other or every day for 10 total days ± 25 or 50 mg/kg TMZ and weight and clinical score was monitored. (**B**) 15 days after intracranial implantation of DB70, BT317 (100mg/kg), Marizomib (50µg/kg) or DMSO (w/v) were injected i.p. at various doses to proteasome activity and Aco2 levels in the tumor, healthy brain and blood at 1 and 4 h. Statistical significance was determined by t-test. * *P* <0.05, ***P* <0.01, ****P* <0.001; n.s., not significant.

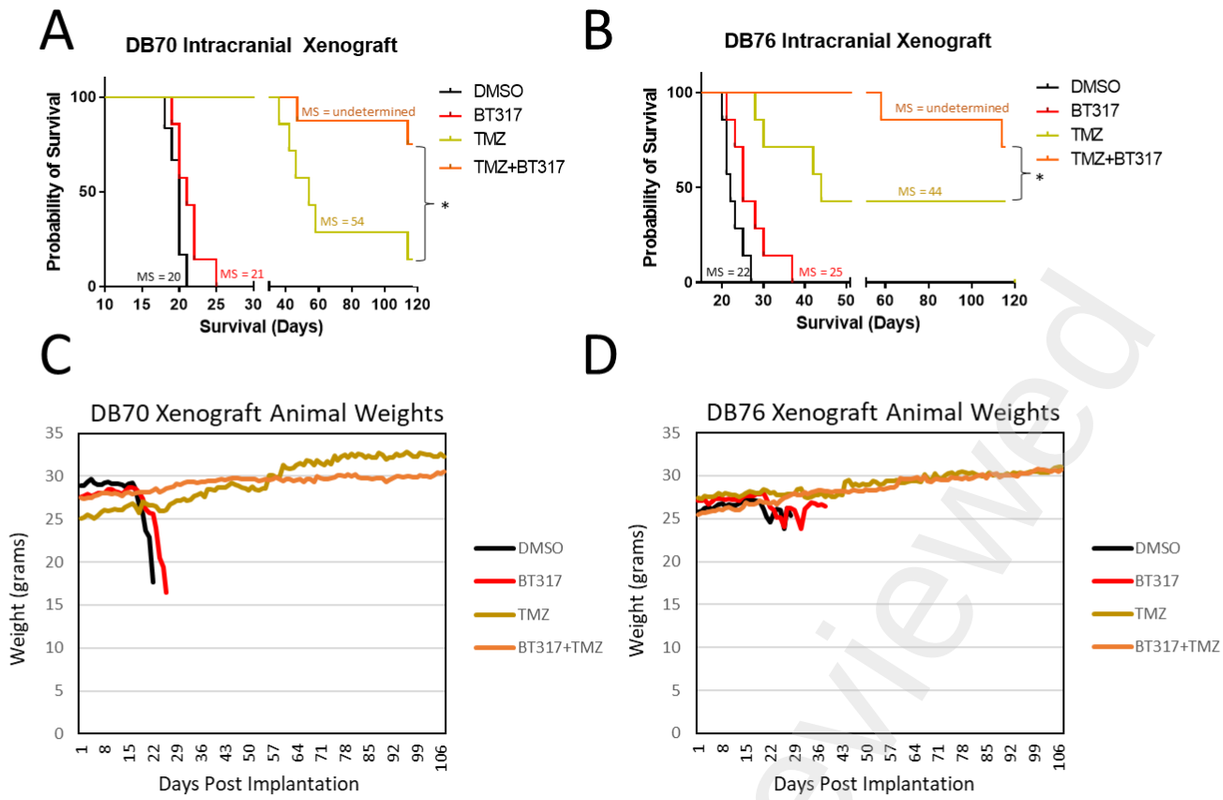

Figure 6. BT317 and Combinatorial BT317 + TMZ Treatment Significantly Improves Survival. (**A**) In the DB70 intracranial model, 100 mg/kg BT317 ± 100 mg/kg TMZ was injected i.p. daily for 5 days starting on day 10 after intracranial implantation. (**B**) The methodology in (A) was applied to assess any survival advantage in the DB76 intracranial xenograft model. Average weights of animals were tracked from post-implantation for (C) DB70 and (D) DB76. Significance was measured n=3 per endpoint).;*p<0.05, **p<0.01, ***p<0.001 ns=not significant. (BT317, n=6; MRZ, n=6, DMSO n=4 per endpoint).

Table 1. Lines for patient-derived samples included in this study.

Patient-derived GSC Lines					
Line	Classification	Grade	IDH1	p53	ATRX
DB70	Astrocytoma	3	Mut	Lost	Lost
DB76	Astrocytoma	4	Mut	Lost	Lost
DB77	Astrocytoma	4	WT	WT	WT
83MES	Glioblastoma	4	WT	N/A	N/A
DB81	Astrocytoma	4	Mut	Lost	Lost

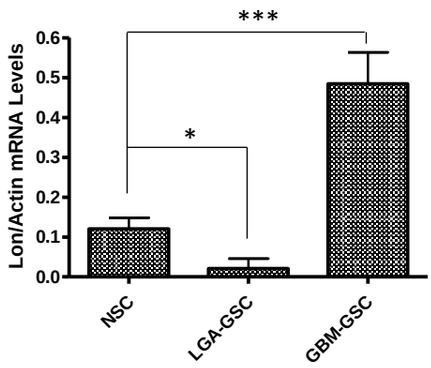

Supplementary Figure S1. LonP1 expression is upregulated in late-stage GBM. (**A**) LonP1 levels were normalized to B-actin via qtPCR for neural stem cells (NSC), low-grade glioma stem cells (LGA-GSC) and glioblastoma glioma stem cells (GBM-GSC). (**B**) Similarly, LonP1 levels were assessed to determine expression in the established D-54 MG, U-251 MG and GBM-GSC lines.

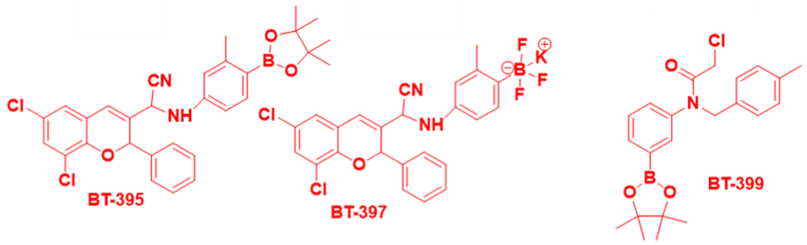

Supplementary Figure S2. CC4 was also used to derive BT395, BT397 and BT399. Chemical structures are as shown.

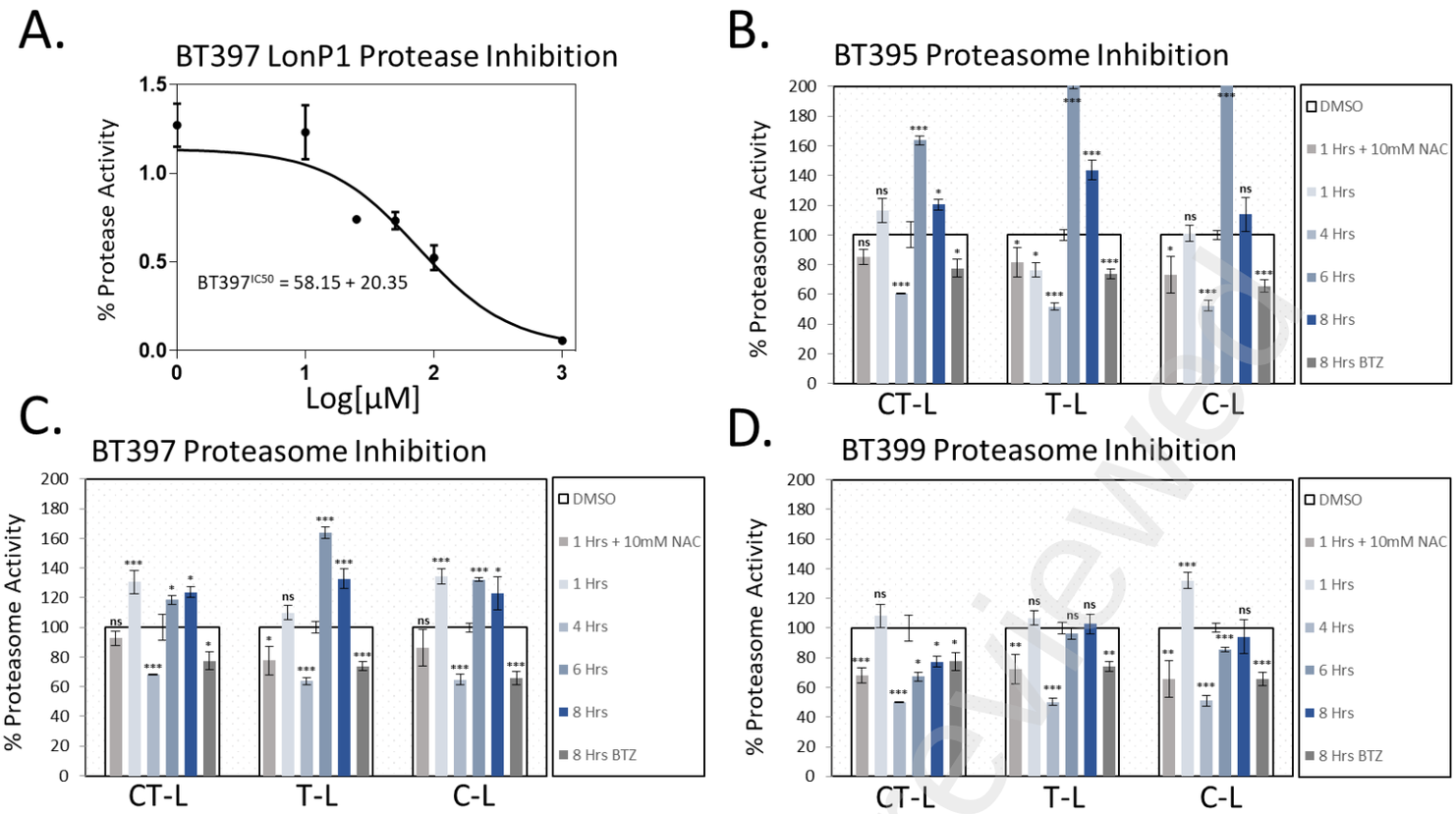

Supplementary Figure S3. BT395, BT397 and BT399 Show Limited Inhibition of LonP1 and Proteasome Activity. (**A**) BT397 was assessed for inhibition of LonP1 protease activity with an IC50 established at 58.15µM (**B-D**) BT395, BT397 and BT399 have variable levels of short-term proteasome inhibition. NAC= N-acetyl Cysteine; BTZ = Bortezomib; CT-L= Chymotrypsin-like activity; T-L = Trypsin-like activity; C-L = Caspase-like activity. Statistical significance was determined by t-test. * P <0.05, **P <0.01, ***P <0.001; n.s., not significant.

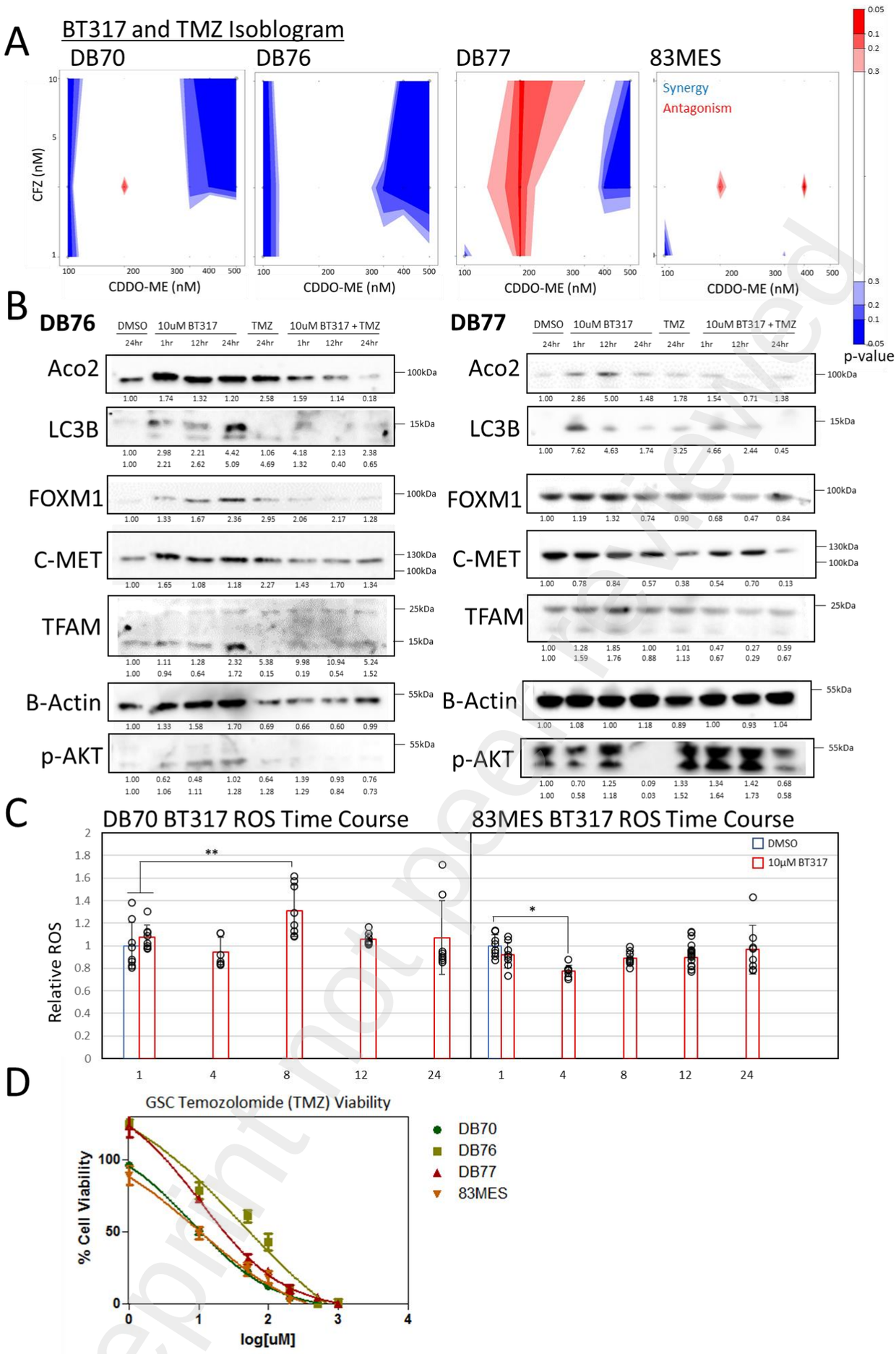

Supplementary Figure S4. BT317 Shows Strong Synergy with TMZ in IDH Mutant GSC Lines. (**A**) Synergy between BT317 and TMZ was evaluated using BIG, with blue representing significant synergy and red representing anergy. (**B**) Protein levels were evaluated at 10μM BT317 ± 10μM TMZ for 1-24 h. (C) Relative sensitivity of each GSC line to TMZ. (D) The DB70 line was subjected to 10μM BT317 ± 10μM TMZ for 24 h and evaluated for colony forming ability 12 days later. (E) ROS levels were analyzed following BT317 treatment at 1, 4, 9, 12 and 24 h. Statistical significance was determined by t-test. * P <0.05, **P <0.01, ***P <0.001; n.s., not significant.

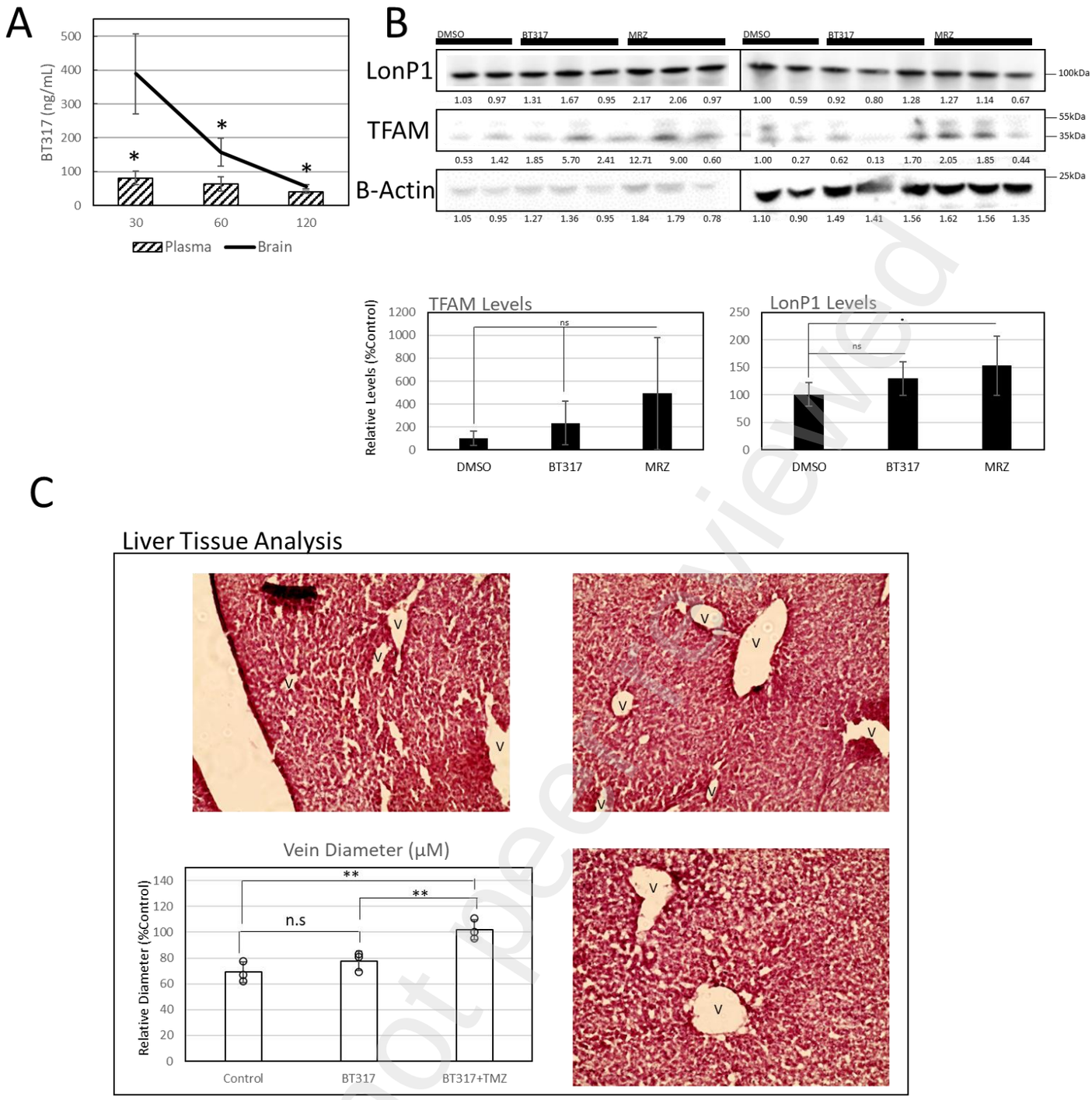

Supplementary Figure S5. BT317 Shows BBB Permeability, Increased LonP1 Inhibition in the Tumor Xenograft and Limited Liver Toxicity . (**A**) Following i.p. injection of 3mg/kg BT317, blood and brain samples were assessed via LC-MS for compound levels. (**B**) Protein levels were evaluated following injection of 100mg/kg of BT317 and 15 days post intracranial xenograft implantation. (**C**) Liver toxicity was evaluated for gross morphological differences and vein diameter following 100mg/kg of BT317 administered daily for 10 days total. Statistical significance was determined by t-test. * P <0.05, **P <0.01, ***P <0.001; n.s., not significant.

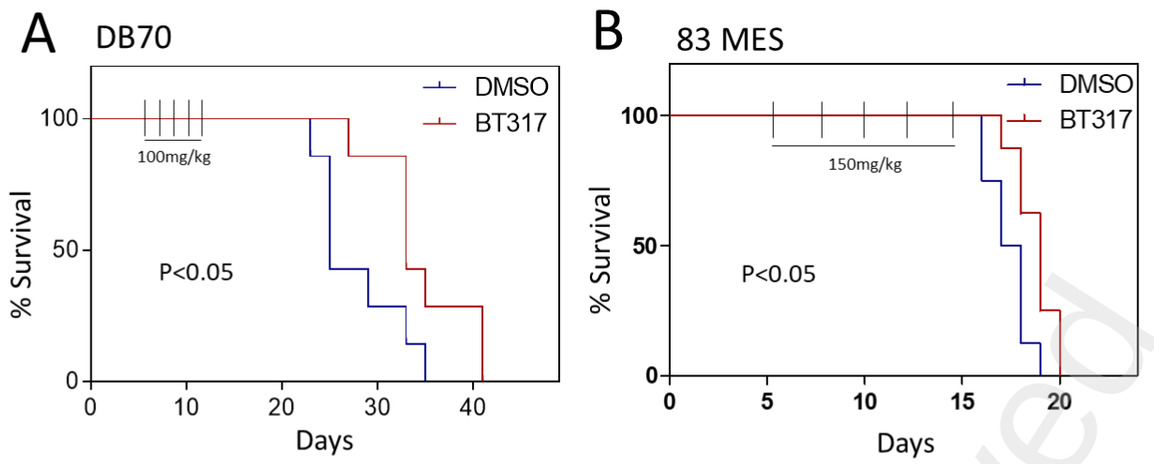

Supplementary Figure S6. BT317 Shows Efficacy Against the 83MES GSC Line. (A) 100 mg/kg in the DB70 or (B) 150 mg/kg BT317 in the 83MES xenograft model was injected i.p. every other day for 5 total doses starting on day 5 after intracranial implantation**.** Significance was measured n=7 per endpoint).;*p<0.05, **p<0.01, ***p<0.001 ns=not significant. (BT317, n=6; MRZ, n=6, DMSO n=4 per endpoint).